The Plant Cell, Vol. 31: 1856–1878, August 2019, www.plantcell.org © 2019 ASPB.

Arabidopsis DGD1 SUPPRESSOR1 Is a Subunit of the Mitochondrial Contact Site and Cristae Organizing System and Affects Mitochondrial Biogenesis[OPEN]

Lu Li,[a] Anastasiya Lavell,[b] Xiangxiang Meng,[a] Oliver Berkowitz,[a] Jennifer Selinski,[a] Allison van de Meene,[c] Chris Carrie,[d] Christoph Benning,[b] James Whelan,[a] Inge De Clercq,[a,1,2] and Yan Wang[a,2]

[a] Department of Animal, Plant and Soil Science, School of Life Science, Australian Research Council Centre of Excellence in Plant Energy Biology, La Trobe University, 5 Ring Road, Bundoora, 3086, Victoria, Australia
[b] MSU-DOE Plant Research Laboratory and Department of Biochemistry and Molecular Biology, Michigan State University, East Lansing, Michigan 48824
[c] School of Biosciences, University of Melbourne, Victoria 3010, Australia
[d] Department Biologie I – Botanik, Ludwig-Maximilians-Universität München, Großhadernerstrasse 2-4, Planegg-Martinsried, 82152, Germany

ORCID IDs: 0000-0002-7410-8706 (L.L.); 0000-0003-1338-2063 (A.L.); 0000-0002-5956-2011 (X.M.); 0000-0002-7671-6983 (O.B.); 0000-0002-1247-7282 (J.S.); 0000-0002-9104-031X (A.v.d.M.); 0000-0002-4240-4674 (C.C.); 0000-0001-8585-3667 (C.B.); 0000-0001-5754-025X (J.W.); 0000-0001-8125-1239 (I.D.C.); 0000-0003-1600-2863 (Y.W.)

Mitochondrial and plastid biogenesis requires the biosynthesis and assembly of proteins, nucleic acids, and lipids. In Arabidopsis (*Arabidopsis thaliana*), the mitochondrial outer membrane protein DGD1 SUPPRESSOR1 (DGS1) is part of a large multi-subunit protein complex that contains the mitochondrial contact site and cristae organizing system 60-kD subunit, the translocase of outer mitochondrial membrane 40-kD subunit (TOM40), the TOM20s, and the Rieske FeS protein. A point mutation in *DGS1*, *dgs1-1*, altered the stability and protease accessibility of this complex. This altered mitochondrial biogenesis, mitochondrial size, lipid content and composition, protein import, and respiratory capacity. Whole plant physiology was affected in the *dgs1-1* mutant as evidenced by tolerance to imposed drought stress and altered transcriptional responses of markers of mitochondrial retrograde signaling. Putative orthologs of Arabidopsis DGS1 are conserved in eukaryotes, including the Nuclear Control of ATP Synthase2 (NCA2) protein in yeast (*Saccharomyces cerevisiae*), but lost in Metazoa. The genes encoding DGS1 and NCA2 are part of a similar coexpression network including genes encoding proteins involved in mitochondrial fission, morphology, and lipid homeostasis. Thus, DGS1 links mitochondrial protein and lipid import with cellular lipid homeostasis and whole plant stress responses.

INTRODUCTION

Mitochondrial biogenesis requires the import of proteins, RNAs, and lipids (Schneider, 2011; Mesmin, 2016; Wiedemann and Pfanner, 2017). The signals and machinery for the import and assembly of proteins are well studied, and one emerging theme is that many proteins are dually targeted to both mitochondria and chloroplasts, highlighting the coordination of function of these organelles (Murcha et al., 2014). Both mitochondria and plastids contain their own genome, but they rely on the import of nuclear-encoded proteins for the replication and expression of their genomes, with many of the involved proteins dually targeted (Elo et al., 2003; Carrie et al., 2009). While some lipids such as cardiolipin (CL) are produced in the mitochondria themselves, mitochondrial lipid biogenesis also depends on the import of lipids from other sites of synthesis, that is, the endoplasmic reticulum (ER) and plastids (Michaud et al., 2017). Lipid transfer/import into mitochondria takes place via contact sites and is nonvesicular in nature. However, little is known about the proteins involved in this process in plants. By contrast, in yeast (*Saccharomyces cerevisiae*) many of the proteins involved have been identified and characterized (Michaud et al., 2017).

In yeast and mammals, the mitochondrial contact site and cristae organizing system (MICOS/mitochondrial inner membrane organizing system/mitochondrial organizing structure), bridging the inner mitochondrial membrane (IMM) and the outer mitochondrial membrane (OMM), has multi-faceted functions in mitochondrial morphology, protein import and abundance, and oxidative phosphorylation as well as lipid biogenesis and content (van der Laan et al., 2016; Schorr and van der Laan, 2018). The components of MICOS are conserved in yeast and humans, with at least six subunits in yeast and nine subunits in humans (van der Laan et al., 2012; Kozjak-Pavlovic, 2017). A phylogenetic analysis for eukaryotes proposed that only two core components of MICOS, MIC60 and MIC10, were conserved in plants (Muñoz-Gómez et al., 2015a, 2015b). A study in Arabidopsis (*Arabidopsis thaliana*)

[1] Current address: VIB Center for Plant Systems Biology, Technologiepark 71, 9052 Ghent, Belgium.
[2] Address correspondence to yan.wang@latrobe.edu.au or I.DeClercq@latrobe.edu.au.
The author(s) responsible for distribution of materials integral to the findings presented in this article in accordance with the policy described in the Instructions for Authors (www.plantcell.org) are: Yan Wang (yan.wang@latrobe.edu.au) and James Whelan (j.whelan@latrobe.edu.au).
[OPEN]Articles can be viewed without a subscription.
www.plantcell.org/cgi/doi/10.1105/tpc.18.00885

IN A NUTSHELL

Background: Plant mitochondria consume 50% of the carbon fixed in photosynthesis. In one pathway, the resulting carbohydrates are converted into energy (ATP) to support growth. Another pathway, where the carbohydrates are consumed in an apparently wasteful respiration pathway producing no energy, is called the alternative respiratory pathway. However, this pathway plays an important role in plant stress responses. Previous work had shown that a mutation in an outer membrane protein, called DGS1, resulted in a lower amount of the wasteful pathway, but the role of this outer membrane protein was unknown.

Question: This study investigated the role of the outer membrane protein and its roles in plant growth and stress responses and evaluated how it affected the abundance of the alternative respiratory pathway.

Findings: We found that in Arabidopsis, the mitochondrial outer membrane DGS1 protein was part of a larger protein complex that is involved in building mitochondrial proteins and lipids, also maintaining mitochondrial structure. Mutation of the protein not only affected mitochondrial function and morphology, but also changed the size of chloroplasts, showing the complexity of regulation of lipid homeostasis in plant cells. This resulted in plants that were more stress tolerant, with less abundance of the wasteful alternative respiratory pathway. The results show that there is a complex regulatory network defining mitochondrial, chloroplast and endoplasmic reticulum function and that altering one organelle has profound impacts on the others, at both the morphological and functional levels.

Next steps: The identification of the existence of this multi-subunit protein complex now offers a way to investigate how organelle biogenesis and lipid homeostasis are coordinated between organelles in plant cells.

revealed that MIC60, interacting with the translocase of the outer mitochondrial membrane (TOM) via the TOM 40-kD subunit (TOM40), forms part of a mitochondrial transmembrane lipoprotein (MTL) complex and affects mitochondrial lipid trafficking (Michaud et al., 2016).

Mitochondrial membrane lipid homeostasis, including biosynthesis and transfer of phospholipids and CL, is controlled by MICOS-mediated membrane contact sites with the ER (Aaltonen et al., 2016; Wideman and Muñoz-Gómez, 2016). In plants, transfer of lipids from plastids to mitochondria has also been detected and is also dependent on physical contact sites (Jouhet et al., 2004). During phosphate (Pi) limitation, phospholipids are replaced by nonphosphorus galactoglycerolipids synthesized in plastids (Härtel et al., 2000), although some galactoglycerolipids are also found in mitochondria under nonlimiting Pi growth conditions (Jouhet et al., 2004; Michaud et al., 2016). The regulatory mechanisms behind determining the amount of mitochondrial galactoglycerolipids are unknown, as are the components responsible for their transfer from plastids to mitochondria.

The bulk of the galactoglycerolipids, that is, mono- and digalactosyldiacylglycerol (MGDG and DGDG, respectively), is synthesized at the inner and outer envelope membranes of the plastid, respectively, and they are highly abundant in the thylakoid membranes of the chloroplast. Galactolipids are unique to photosynthetic membranes under normal conditions. However, in response to Pi deprivation, galactolipids are exported to extraplastidic membranes (Moellering and Benning, 2011). Galactolipid biosynthesis is performed in the chloroplast envelope membranes by a set of MGDG synthases (MGDs) that catalyze the formation of MGDG followed by DGD synthases (DGDs) that use MGDG to form DGDG (Benning and Ohta, 2005). *MGD1* and *DGD1* are constitutively expressed, while *MGD2, MGD3*, and *DGD2* are induced in response to Pi limitation (Awai et al., 2001; Kelly and Dörmann, 2002). To identify regulators of galactoglycerolipid biosynthesis in response to Pi deprivation, a genetic suppressor screen was conducted in the Arabidopsis *dgd1* mutant background. A *dgd1* suppressor mutant allele (*dgd1 suppressor 1*, *dgs1-1*) was identified that constitutively activated the DGD1-independent pathway for DGDG biosynthesis (Xu et al., 2003, 2008). The affected protein, DGS1, has two membrane-spanning domains and was localized to the OMM as part of a larger protein complex (Xu et al., 2008; Moellering and Benning, 2010). It contains a conserved domain also found in a yeast protein identified in a genetic screen for assembly of the ATP synthase complex Nuclear Control of ATP Synthase2 (NCA2; Camougrand et al., 1995).

In this study, we demonstrated that the OMM protein DGS1 is a novel subunit of MICOS in plants. We showed that DGS1 constituted part of a multi-subunit protein complex with MIC60. A point mutation of DGS1 affected chloroplast and mitochondrial lipid content and composition as well as mitochondrial biogenesis and function, which were also the effects of MICOS in yeast and mammals (van der Laan et al., 2016; Schorr and van der Laan, 2018). DGS1 was conserved across eukaryotes but absent from Metazoa and Alvaeolata. NCA2, the yeast putative ortholog of DGS1, and DGS1 had a similar coexpression network including proteins involved in mitochondrial biogenesis.

RESULTS

DGS1 Is Present in a Multi-Subunit Protein Complex with MIC60, TOM40, TOM20s, and RISP

Using immunoblotting following blue-native PAGE (BN-PAGE), immunoprecipitation, and crosslinking with the membrane-permeable chemical crosslinker disuccinimidyl glutarate (DSG), DGS1 was found to be present in a multi-subunit protein complex that contains MIC60, TOM40, TOM 20-kD subunits (TOM20s), and the Rieske FeS protein (RISP) of the cytochrome (Cyt) bc_1 complex (Figure 1). Mass spectrometry of excised bands revealed that DGS1 comigrated with MIC60 in the oxidative phosphorylation complexes complex V, complex III, and complex F_1 (Figure 1A; Supplemental Data Set 1). The immunoblot following BN-PAGE

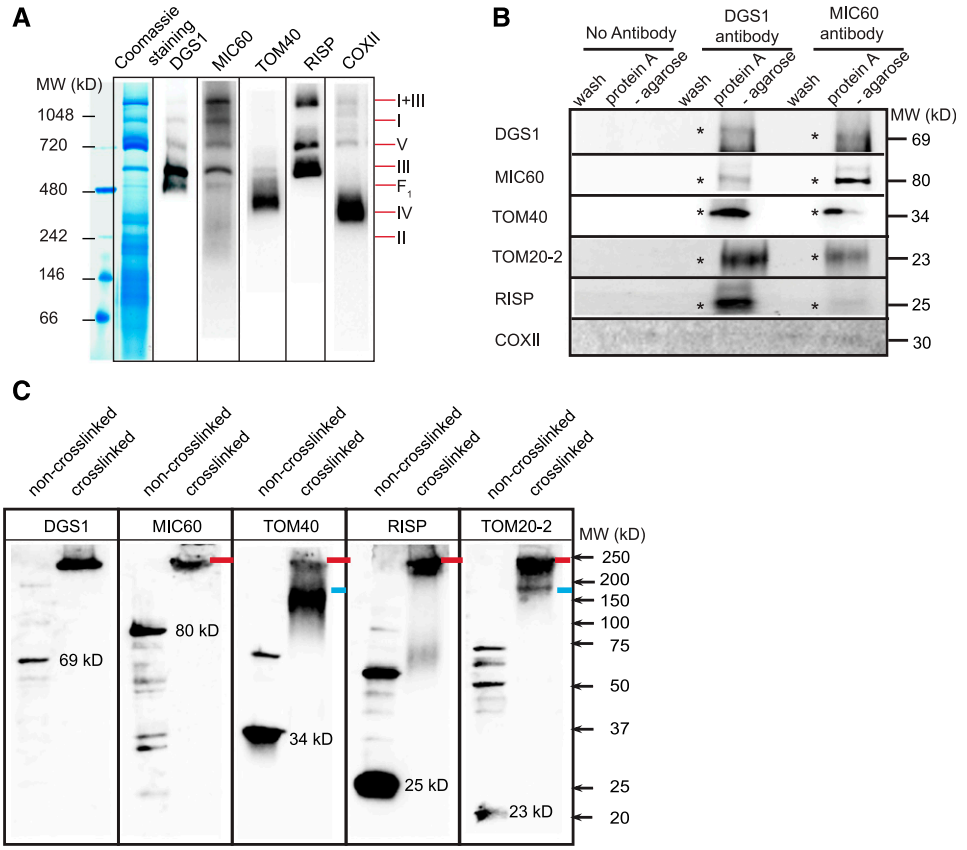

Figure 1. DGS1 Is Present in a Large Multi-Subunit Protein Complex with MIC60, TOM40, TOM20s, and RISP.

(A) Immunodetection of DGS1, MIC60, TOM40, complex III subunit RISP, and complex IV subunit COXII in total mitochondrial proteins separated by BN-PAGE. Coomassie blue staining was performed showing the distribution of supercomplex I+III, complex F_1, and complexes I to V. MW, molecular weight.
(B) Mitochondrial proteins from the wild-type (Col-0) plants were incubated without or with antibodies raised against DGS1 and MIC60. The wash and protein A-agarose pellet fractions were resolved by SDS-PAGE and immunodetected with antibodies as shown. The interaction between proteins is indicated by asterisks, and the corresponding molecular weight (MW) for each protein is indicated in kDa
(C) Mitochondrial proteins incubated with or without crosslinker were resolved by SDS-PAGE, followed by immunodetection. Red lines indicate proteins that exist in the same complex with DGS1, while blue lines indicate association with another complex. The size of non-crosslinked protein is indicated in each panel. MW, molecular weight.

revealed the majority of DGS1 was detected in complex III (Figure 1A), while MIC60 comigrated with a variety of respiratory complexes (Figure 1A). Immunoprecipitation using a DGS1 antibody pulled down MIC60, TOM40, TOM20-2, and RISP, while the MIC60 antibody pulled down DGS1, TOM40, TOM20-2, and RISP (Figure 1B). RISP was not efficiently pulled down by MIC60. This may be due to the fact that while the majority of the DGS1 protein comigrates with complex III (Figure 1A), MIC60 was found in a number of protein complexes (Figure 1A; Michaud et al., 2016); thus, only a fraction of the MIC60 antibody recognized MIC60 that was in a complex with RISP. The interaction of MIC60 with the TOM complex is in agreement with a previous report that showed interaction between MIC60 and TOM40 (Michaud et al., 2016). Cytochrome oxidase II (COXII), a subunit of complex V, was not pulled down by either DGS1 antibody or MIC60 antibody, presented as a negative control (Figure 1B).

To further confirm the interactions, purified intact mitochondria were treated with membrane-permeable chemical crosslinker DSG to capture transient, semi-stable, and stable association of proteins. DSG is a crosslinker that uses the amine-reactive *N*-hydroxysuccinimide ester group, linking amino to amino groups at <8 Å in proximity. After crosslinking, centrifugation at 500 relative centrifugal force (RCF) for 2 min was performed to pellet and remove aggregated proteins. The supernatant (crosslinked sample) was analyzed by SDS-PAGE and immunodetection. The untreated mitochondria (non-crosslinked sample) were loaded beside as size control. Thus, crosslinked and non-crosslinked samples contained different amounts of mitochondrial input protein and cannot be compared for intensity. Therefore, we rather determined whether the target proteins could be crosslinked into a complex with DGS1. DGS1, MIC60, TOM40, TOM20-2, and RISP were crosslinked by DSG in a complex with an apparent molecular mass of 250 kD (Figure 1C, indicated with a red line). TOM40 and TOM20-2 were also present in another complex with a molecular mass of ~200 kD, likely representing the TOM complex (Figure 1C, indicated with a blue line). Taken

together, DGS1 interacts with MIC60, RISP, TOM40, and TOM20-2, forming a multi-subunit protein complex.

The *dgs1-1* Mutation Alters the Multi-Subunit Complex

To determine the function of the DGS1 protein in the multi-subunit complex, eight different transgenic and mutant lines of Arabidopsis were functionally characterized (Figure 2). The *dgs1-1* point mutation line *dgs1-1* was from the original study identifying the DGS1 protein (Moellering and Benning, 2010), which has a change in a single amino acid from Asp to Asn at position 457 close to the predicted transmembrane region (Figure 2A). The *dgs1* T-DNA insertion line *dgs1-2*, containing a T-DNA in the third exon of the *dgs1* gene, was confirmed by PCR and DNA sequencing (Figure 2A) and had a complete loss of DGS1 protein as indicated by immunoblotting (Figure 2B). This line was transformed with the sequences encoding the wild-type DGS1 and the dgs1-1 mutant protein, respectively, under the control of a 35S *Cauliflower mosaic virus* promoter to generate complemented (Comp) lines with different levels of the native and mutated DGS1 protein. A summary of the mutants/Comp lines is listed in Supplemental Data Set 2. The *DGS1* Comp low (L) line produced the DGS1 protein at a low level, half of the DGS1 level in the wild-type plants; the *DGS1* Comp high (H) line produced the DGS1 protein at a high level, more than 10 times of the DGS1 level in the wild-type plants (Figure 2B); the *dgs1-1* Comp (L) expressed the *dgs1-1* mutant coding sequence producing the dgs1-1 mutant protein close to the DGS1 level in the wild-type plants; *dgs1-1* Comp (M [moderate]) expressed the *dgs1-1* mutant coding sequence producing 10 times more dgs1-1 mutant protein than the wild-type DGS1 levels; and *dgs1-1* Comp (H1) and *dgs1-1* Comp (H2) expressed the *dgs1-1* mutant coding sequence producing 20 times more dgs1-1 mutant protein than the wild-type DGS1 levels (Figure 2B).

To determine whether the abundance of MIC60, TOM40, TOM20s, and RISP was affected in these lines, mitochondria were purified from the eight mutant/Comp lines and the wild-type plants (Arabidopsis Columbia 0 ecotype [Col-0]), and mitochondrial proteins were quantified by immunoblotting. Arabidopsis contains four genes that encode TOM20 proteins, but only three are expressed: *TOM20-2*, *TOM20-3*, and *TOM20-4* (Lister et al., 2007). The amount of all TOM20 proteins was observed to be reduced by ~50% in the *dgs1-1* line and *dgs1-1* Comp (L) line (Figure 2B). MIC60 also displayed a 10% to 15% reduction in abundance in the *dgs1-1* line and *dgs1-1* Comp (L) line, but this reduction was only statistically significant in the *dgs1-1* Comp (L) line (Figure 2B). The other two components of the multi-subunit complex, TOM40 and RISP, remained unchanged in the *dgs1-1* line and the *dgs1-1* Comp (L) line and were also unchanged in the lines overexpressing the wild-type DGS1 protein, indicating that the dgs1-1 mutant protein had a specific effect on MIC60 and TOM20 proteins. Finally, in both the *dgs1-1* Comp (M) and (H) lines with high levels of dgs1-1 mutant protein, all the components were reduced in abundance (Figure 2B). The abundance of COXII that does not interact with the complex components was not changed in any line (Figure 2B).

The submitochondrial location of MIC60, TOM40, TOM20-2, RISP, and DGS1 was determined by treating intact and outer membrane–ruptured mitochondria with increasing amounts of protease K, with uncoupling protein and Cyt *c* as controls for inner membrane and intermembrane space location, respectively. As expected, uncoupling protein was resistant to protease K with intact mitochondria and outer membrane–ruptured mitochondria, and no difference was observed in the mutant lines compared with Col-0 (Figure 2C). Cyt *c* was not detected in outer membrane–ruptured mitochondria isolated from Col-0, *dgs1-2*, and plants complemented with the native DGS1 protein, showing complete rupture of OMM during swelling, with complete release of Cyt *c* into solution and thus it was absent from the pellet (Figure 2C). However, in *dgs1-1*, *dgs1-1* Comp (L), (M), and (H) plants, some Cyt *c* was still detectable in outer membrane–ruptured mitochondria (Figure 2C). This indicates that the OMM is not completely ruptured in *dgs1-1*,*dgs1-1* Comp (L), (M), and (H) lines during the swelling-shrinking procedure. The reason is proposed to be that the structure of MICOS bridging the OMM and IMM has been changed due to the *dgs1-1* mutation. Similarly, MIC60 was accessible to protease K in outer membrane–ruptured mitochondria from Col-0, *dgs1-2*, and plants complemented with the native DGS1 protein (Figure 2C), as expected for an intermembrane space–exposed protein (Michaud et al., 2016). Similar to Cyt *c*, MIC60 was still detectable with *dgs1-1*, *dgs1-1* Comp (L), (M), and (H) plants (Figure 2C). The opposite was observed with RISP. While it was totally protected from digestion in mitochondria isolated from Col-0, some digestion was observed in the *dgs1-1*, *dgs1-1* Comp (L), (M), and (H) plants upon rupturing the outer membrane (Figure 2C). TOM20-2 and TOM40 are outer membrane proteins. They were digested by protease K both in intact mitochondria and outer membrane–ruptured mitochondria, and no difference was observed between the lines (Supplemental Figure 1). DGS1 showed a similar sensitivity as TOM20-2, with no difference among the lines (Figure 2C). The ~220 amino acid domain (75 to 297 amino acids) at the N-terminal side of the first transmembrane domain, against which the DGS1 antibody was produced, was digested by protease K. This result suggested an N-out and C-out topology for DGS1 with a loop in the intermembrane space and two transmembrane regions (Figures 2A and 2C). This result also places the mutation in DGS1-1 on the intermembrane space side of the protein, potentially affecting mitochondrial proteins that may interact with DGS1. Thus, the dgs1-1 mutant protein decreases the protease accessibility of MIC60 and Cyt *c*, while making RISP more accessible, even though the dgs1-1 mutant protein is present at the wild-type levels.

To determine whether the dgs1-1 mutant protein affected the multi-subunit complex containing DGS1, MIC60, TOM40, TOM20s, and RISP (Figure 1C), mitochondrial proteins from *dgs1-1* Comp (L) plants were crosslinked as outlined above. The abundance of DGS1, MIC60, TOM40, and TOM20-2 in the crosslinked 250-kD complex was significantly reduced in *dgs1-1* Comp (L) plants, compared with Col-0 (Figure 2D, indicated with red asterisks). By contrast, the abundance of RISP in the crosslinked 250-kD complex was increased in *dgs1-1* Comp (L) plants, compared with Col-0 (Figure 2D, indicated with blue asterisks). Based on these results, we conclude that the interaction between DGS1, MIC60, TOM40, TOM20, and RISP proteins is disturbed when dgs1-1 mutant protein is expressed at native levels.

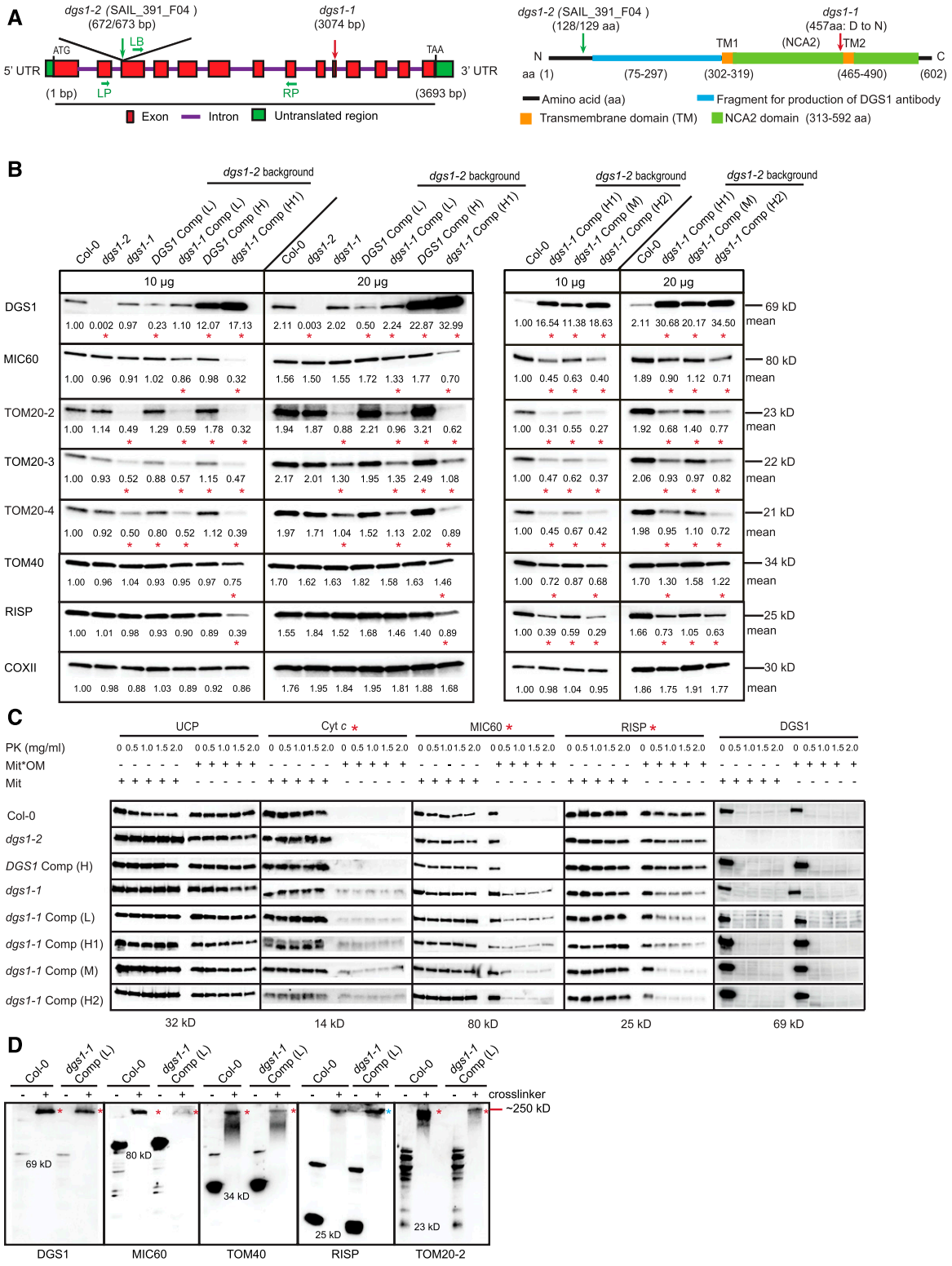

Figure 2. A Single Point Mutation in DGS1 Alters the Multi-Subunit Complex.

(A) Schematic gene (left) and protein (right) model of DGS1. The position of the ethyl methanesulfonate point mutation and T-DNA insertion is indicated. Primers used for screening of homozygous plants are indicated as left primers (LP), right primer (RP), and left border primer (LB; Supplemental Data Set 6).

The *dgs1-1* Mutation Alters Mitochondrial Size

To determine whether disturbing the multi-subunit complex affects organellar distribution, morphology, or size, confocal and transmission electron microscopy was performed. Plant mitochondria exist as a dynamic tubular reticulate network that is maintained by a balance of fusion and fission (Palmer et al., 2011; Rose and McCurdy, 2017). To assess overall morphology in terms of size, constructs for the transient expression of alternative oxidase (AOX)-green fluorescent protein (GFP; targeted to mitochondria) and KDEL-yellow fluorescent protein (YFP; targeted to the ER) were transiently transformed into protoplasts isolated from Col-0, *DGS1* Comp (L), *DGS1* Comp (H), *dgs1-1* Comp (L), *dgs1-1* Comp (M), and *dgs1-1* Comp (H1) plants. In Col-0 and plants complemented with the native DGS1 protein, mitochondria surrounded chloroplasts, as is typical in protoplasts (Duchêne et al., 2005). By contrast, in *dgs1-1* Comp (L), the red fluorescent protein (RFP) signal showed that mitochondria were significantly enlarged, forming a doughnut shape or oval structures (Figure 3A). While these structures varied in size, there were many mitochondria that were much greater in diameter than any mitochondrial structures observed in Col-0, *DGS1* Comp (L), and *DGS1* Comp (H) lines. With increased levels of the dgs1-1 mutant protein, a further increase of mitochondrial size was observed in *dgs1-1* Comp (M) and *dgs1-1* Comp (H) plants (Figure 3A). Enlargement of mitochondria was also observed in yeast *mic60* strains and Arabidopsis *mic60* knockout lines (Rabl et al., 2009; Michaud et al., 2016). A corresponding reduction in chloroplast size was observed with increasing amounts of the dgs1-1 mutant protein (Figure 3A). With dgs1-1 mutant protein levels similar to native levels of the DGS1 wild-type protein, the *dgs1-1* Comp (L) line had a significant reduction in chloroplast diameter (Figure 3A). By contrast, with higher levels of the dgs1-1 mutant protein, mitochondrial size and diameter were equal to those of chloroplasts in the *dgs1-1* Comp (M) and *dgs1-1* Comp (H) lines (Figure 3A). The YFP signal showed that the ER structure was also affected in *dgs1-1* Comp (L), *dgs1-1* Comp (M), and *dgs1-1* Comp (H) lines (Figure 3A). Together, the shapes of mitochondria, chloroplast, and ER were all affected in the lines expressing the dgs1-1 mutant protein.

Transmission electron microscopy was performed to investigate whether the internal morphology of mitochondria was altered (Figure 3B). As transmission electron microscopy allows morphology to be assessed at the nanometer level, it will allow assessment of changes in cristae morphology and/or number. Sections obtained from the wild-type (Col-0) plants revealed mitochondria with numerous infoldings of the inner membrane that represent cristae. By contrast, in the *dgs1-1* line, *dgs1-1* Comp (L) line, and *dgs1-1* Comp (H1) line, consistently fewer cristae could be detected (Figure 3B). The alteration of the inner membrane morphology with fewer cristae provides a possible reason why Cyt *c* was not completely released from OMM-ruptured mitochondria in the *dgs1-1*, *dgs1-1* Comp (L), Comp(M), and and Comp (H) lines observed above (Figure 2C). Thus, a change in a MICOS subunit in Arabidopsis results in changes in cristae abundance as described for yeast and mammalian MICOS systems (van der Laan et al., 2016; Schorr and van der Laan, 2018).

The *dgs1-1* Mutation Alters Mitochondrial Lipid Composition

As MIC60 in Arabidopsis has been shown to play a role in lipid trafficking (Michaud et al., 2016) and the *dgs1-1* mutant was identified based on its altered lipid composition (Xu et al., 2008), the lipids of mitochondria and chloroplasts in *dgs1-1*, *dgs1-1* Comp (L), and *dgs1-1* Comp (H1) plants were profiled. The chloroplast lipid analysis showed that the total fatty acid profiles of Arabidopsis lines expressing the dgs1-1 mutant protein had a dose-dependent decrease in 16:3 and 18:3 acyl chain abundance and a corresponding relative increase in 16:0, 18:1, and 18:2 acyl chain abundance (Figure 4A). The decrease in 16:3 methyl esters abundance can be attributed primarily to the change in MGDG acyl composition. As the predominant chloroplast lipid, it typically carries 16:3 and 18:3 acyl chains in a 1:2 ratio, respectively, at the *sn*-1 and *sn*-2 positions of the glycerol backbone. Additionally, the observed decrease in total abundance of 18:3 acyl chains in the chloroplast lipids was due to a decreased abundance of 18:3 acyl in DGDG, phosphatidylglycerol (PG), and sulfoquinovosyldiacylglycerol (Figure 4A).

In mitochondria, the most abundant lipids, CL, phosphatidylcholine (PC), and phosphatidylethanolamine (PE), all showed a significant decrease in 18:2 acyl chain abundance that appeared dependent on the abundance of the dgs1-1 mutant protein (Figure 4B). Additionally, there was a corresponding increase in the relative amount of 16:0 acyl chains esterified to those lipids (Figure 4B). The total lipid profiles showed a significant decrease in the relative amount of CL with increased levels of the dgs1-1 mutant protein, while the relative amount of PC was increased (Figure 4B).

Figure 2. (continued).

Two transmembrane domains, the NCA2 domain and the fragment used for the generation of the DGS1 antibody, are indicated in different colors. aa, amino acid; C, C terminus; N, amino terminus; UTR, untranslated region.

(B) Protein abundance of DGS1, MIC60, TOM20s, TOM40, RISP, and COXII was determined by immunoblot analysis of mitochondrial proteins isolated from the wild-type (Col-0), *dgs1-1*, and *dgs1-2* mutant lines as well as several lines expressing the dgs1-1 mutant protein. Ten micrograms and 20 μg of mitochondrial proteins were loaded to ensure linearity of detection. Mean values are shown for three biological replicates. P-value ≤ 0.05 from a Student's *t* test is indicated with red asterisks.

(C) Freshly isolated mitochondria (Mit) and outer membrane–ruptured mitochondria (Mit*OM) from the wild-type (Col-0), *dgs1-1*, and *dgs1-2* mutant lines as well as several lines expressing the dgs1-1 mutant protein were treated with protease K (PK) at different concentrations, followed by immunodetection. Proteins displaying altered PK sensitivity are indicated with red asterisks.

(D) Crosslinked and non-crosslinked mitochondrial proteins from the wild-type (Col-0) plants and *dgs1-1* Comp (L) plants were resolved by SDS-PAGE, followed by immunodetection. Red asterisks indicate the protein abundance in the crosslinked complex was reduced in the *dgs1-1* Comp (L) line, while the blue asterisk indicates the protein abundance was increased. The size of non-crosslinked protein is indicated in each panel.

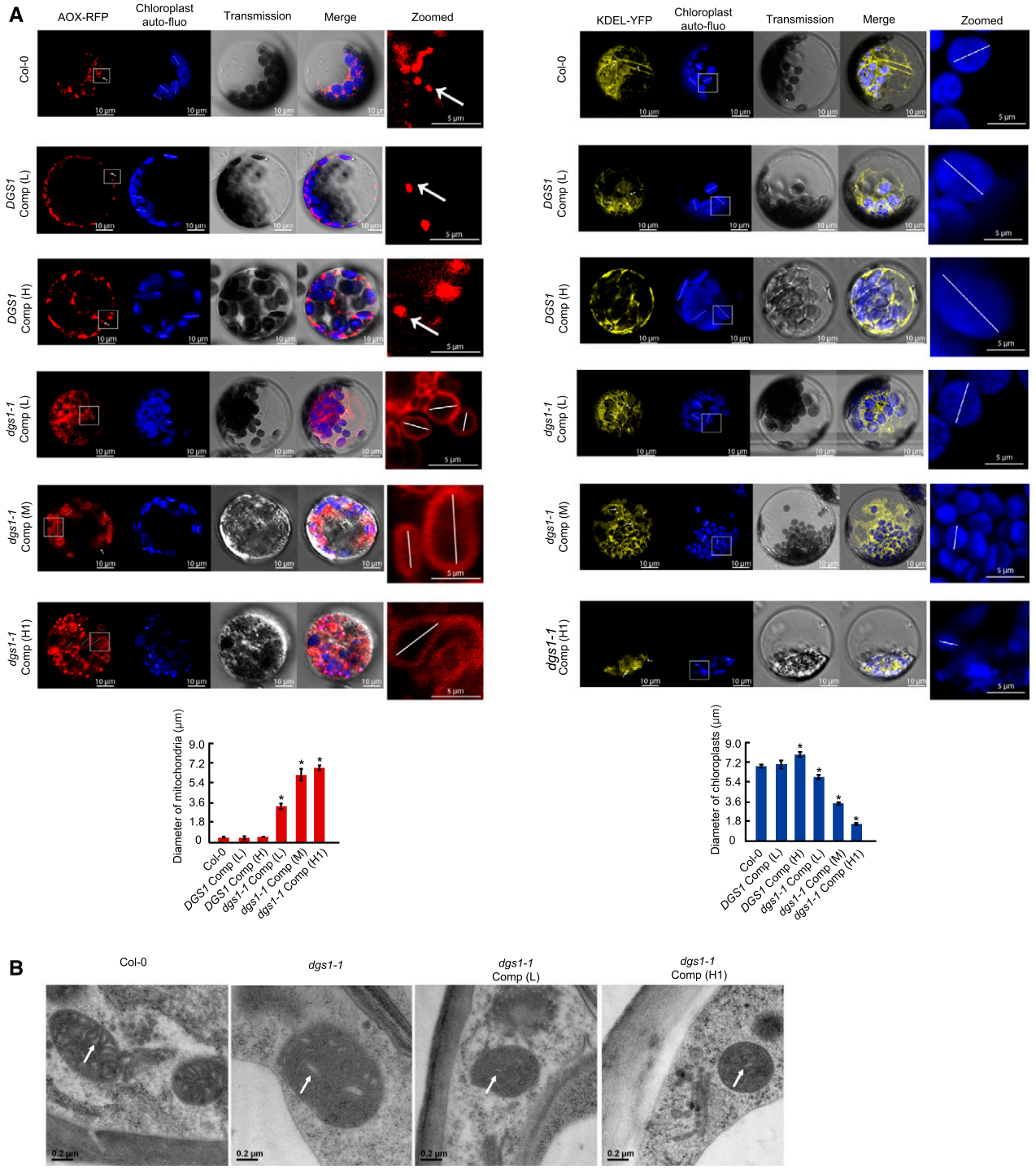

Figure 3. The *dgs1-1* Mutation Alters Mitochondrial Size.

(A) Protoplasts isolated from the indicated genotypes were transiently transformed with AOX-RFP (mitochondria targeting construct) and KDEL-YFP (ER targeting construct), respectively. Chloroplasts were observed using chlorophyll auto-fluorescence (auto-fluo). Bars = 10 μm. The rectangle areas were zoomed in to show the altered mitochondrial and chloroplast size. Bars = 5 μm. The diameter of chloroplasts and mitochondria were averaged from 30 protoplast cells, and significant differences were assessed using Student's *t* test with $P \leq 0.05$ indicated by asterisks. The white line(s) indicates the diameter measurement used.

(B) Electron microscopy images of mitochondria cross sections from leaf tissue of the Col-0, *dgs1-1* line, *dgs1-1* Comp (L) line, and *dgs1-1* Comp (H1) line. The internal cristae membranes are indicated with white arrows. Bars = 0.2 μm.

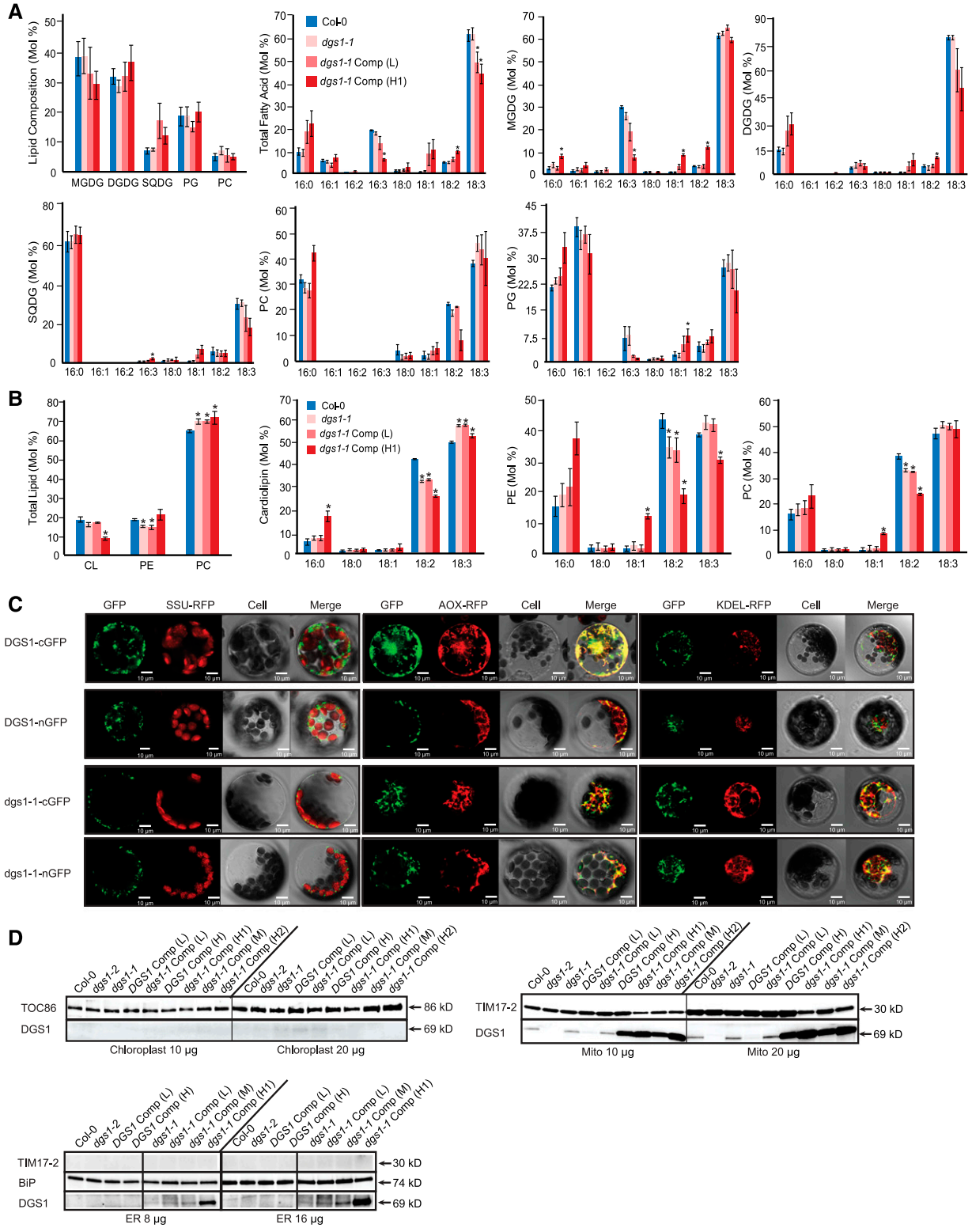

Figure 4. The *dgs1-1* Mutation Alters Mitochondrial Lipid Composition.

(A) and **(B)** Lipid analysis by GLC of chloroplasts **(A)** and mitochondria **(B)** extracted from the wild-type (Col-0) and *dgs1* mutant lines. Significant differences in relative composition of each acyl chain and total lipids were determined by Student's *t* test with P-value ≤ 0.05 ($n = 3$) indicated by asterisks. Error bars indicate SE. SQDG, sulfoquinovosyldiacylglycerol.

Analysis of total leaf lipids revealed a dose-dependent decrease in 16:3 acyl chain abundance with a relative increase in 18:1 acyl chain abundance (Supplemental Figure 2A). The total leaf DGDG and MGDG showed the same trend as in chloroplasts as would be expected. A decrease in the 18:2 acyl chains in PC and 18:3 acyl chains in PG was accompanied by a relative increase in 18:1 acyl chains. For PE, a decrease in 18:2 chains was also observed in total leaf lipid profiles such as in mitochondria, but an increase in 18:3 acyl chains was observed in total lipids that was not observed for mitochondrial lipids. For PC, the same pattern was observed in lipids from mitochondria and total leaf lipids: a decrease in 18:2 acyl chains with a corresponding increase in the 18:1 acyl chains. Thus, the total leaf lipid composition was changed, but the largest effect was observed with mitochondria and chloroplast lipids. It should be noted that in the line with the highest amount of dgs1 mutant protein, galactolipids MGDG and DGDG and oligogalactolipids were observed to be associated with the mitochondrial fraction above the wild-type background levels (Supplemental Figure 2B). Typically, MGDG and oligogalactolipids are restricted to chloroplasts. The latter are formed under stress conditions by the action of SFR2 (Moellering et al., 2010).

To interpret why the mitochondrial DGS1 protein could affect chloroplast lipid composition, the locations of the DGS1 wild-type protein and the dgs1-1 mutant protein were investigated. The constructs expressing the DGS1 wild-type protein and the dgs1-1 mutant protein tagged with C-terminal GFP or N-terminal GFP were transiently transformed into the wild-type protoplasts, with pea small subunit of Rubisco (SSU)-RFP as chloroplast control, AOX-RFP as mitochondrial control, and KDEL-RFP as ER control. The fluorescence imaging revealed that the DGS1 protein was located in mitochondria, while the dgs1-1 mutant protein was associated with both mitochondria and the ER (Figure 4C). To confirm these results, chloroplast, mitochondria, and ER fractions were isolated from Col-0, *dgs-1*, *dgs1-2* mutant, and Comp lines, followed by immunoblotting with the DGS1 antibody. In Col-0, the DGS1 wild-type protein was only detectable in mitochondria (Figure 4D). By contrast, in the mutant lines that expressed the dgs1-1 mutant protein, it was detectable in both mitochondria and the ER (Figure 4D), even when expressed at native levels. No DGS1 protein or dgs1-1 mutant protein was detected in chloroplasts (Figures 4C and 4D).

The *dgs1-1* Mutation Affects Mitochondrial Protein Abundance, Protein Import, and Alternative Respiratory Capacity

MICOS was reported to affect mitochondrial protein import and respiration in yeast and mammals (Schorr and van der Laan, 2018). To determine whether disturbing the multi-subunit complex by the presence of dgs1-1 mutant protein had the same effects in plants, the abundance of various proteins involved in protein import and respiration was determined. Notably, the *dgs1-2* null mutant did not affect the abundance of any protein or the activity of the respiratory chain (Figures 5A and 5B). However, both the *dgs1-1* mutant and the *dgs1-1* Comp (L) line with protein levels comparable to the wild type showed decreased abundance of an outer membrane (OM) β-barrel protein in plant mitochondria (OM47; Li et al., 2016b), TIM44, and AOX (Figure 5A). The consistent decrease in abundance of TOM20s (Figure 2B), OM47, TIM44, and AOX (Figure 5A) in all lines expressing the dgs1-1 mutant protein indicates that the mutated dgs1-1 protein has an effect on specific proteins or pathways. However, it is worth noting that the abundance of almost all mitochondrial proteins tested showed a decrease of various degrees in lines expressing medium and high levels of the dgs1-1 mutant protein (Figure 5A). We consider that this is an unspecific effect that may result from the altered mitochondrial lipid content and high level of dgs1-1 mutant protein (Figure 4A), and such decreases were not observed in the lines expressing high levels of the DGS1 wild-type protein (Figure 5A). Along with the alterations in abundance of mitochondrial proteins, a similar trend was observed in respiratory capacity (Figure 5B). The activity of the alternative oxidase pathway as assessed by the reduction in *n*-propyl gallate–sensitive oxygen uptake was specifically inhibited by the expression of the dgs1-1 mutant protein (Siedow and Girvin, 1980). This reduction in activity of the alternative pathway was observed even when the dgs1-1 mutant protein was expressed at physiological levels. A general reduction in total respiration and respiration through the Cyt *c* oxidase pathway, and oxygen consumption driven by oxidation of substrates by complex I and complex II was observed only with high levels of dgs1-1 mutant protein, but not the DGS1 wild-type protein (Figure 5B).

To examine whether mitochondrial protein import ability was affected by the presence of the dgs1-1 mutant protein, in vitro import of radiolabeled plant mitochondrial precursor proteins into mitochondria isolated from Col-0, *dgs1-1* Comp (L), and *dgs1-1* (H1) plants was performed (Figure 5C). For the precursor protein of AOX, representing the general import pathway, and the adenine nucleotide carrier ANT, representing the carrier import pathway, strongly reduced import rates were observed with both *dgs1-1* Comp (L) and *dgs1-1* Comp (H) plants, compared with Col-0 (Figure 5C), indicating an impairment of mitochondrial protein import by the presence of the dgs1-1 mutant protein.

Higher Drought Stress Tolerance in *dgs1-1* Mutant Plant Lines

Quantitative phenotypic analysis revealed that the plants expressing the dgs1-1 mutant protein were smaller than Col-0 plants

Figure 4. (continued).

(C) Construct expressing full-length DGS1 protein or dgs1-1 mutant protein with C- or N-terminal GFP was transiently transformed into protoplasts isolated from Arabidopsis Col-0 plants. Pea small subunit of Rubisco (SSU)-RFP (targeting to chloroplasts), AOX-RFP (targeting to mitochondria), or KDEL-RFP (targeting to ER) was cotransformed as control. Bars = 10 μm.

(D) Proteins of chloroplasts, mitochondria, and ER isolated from Col-0 and *dgs1* mutant plants were separated by SDS-PAGE and followed by immunoblotting using the DGS1 antibody, the TOC86 antibody as a chloroplast marker, the TIM17-2 antibody as a mitochondria marker, and BiP as an ER marker. BiP, lumenal-binding protein; Mito, mitochondria .

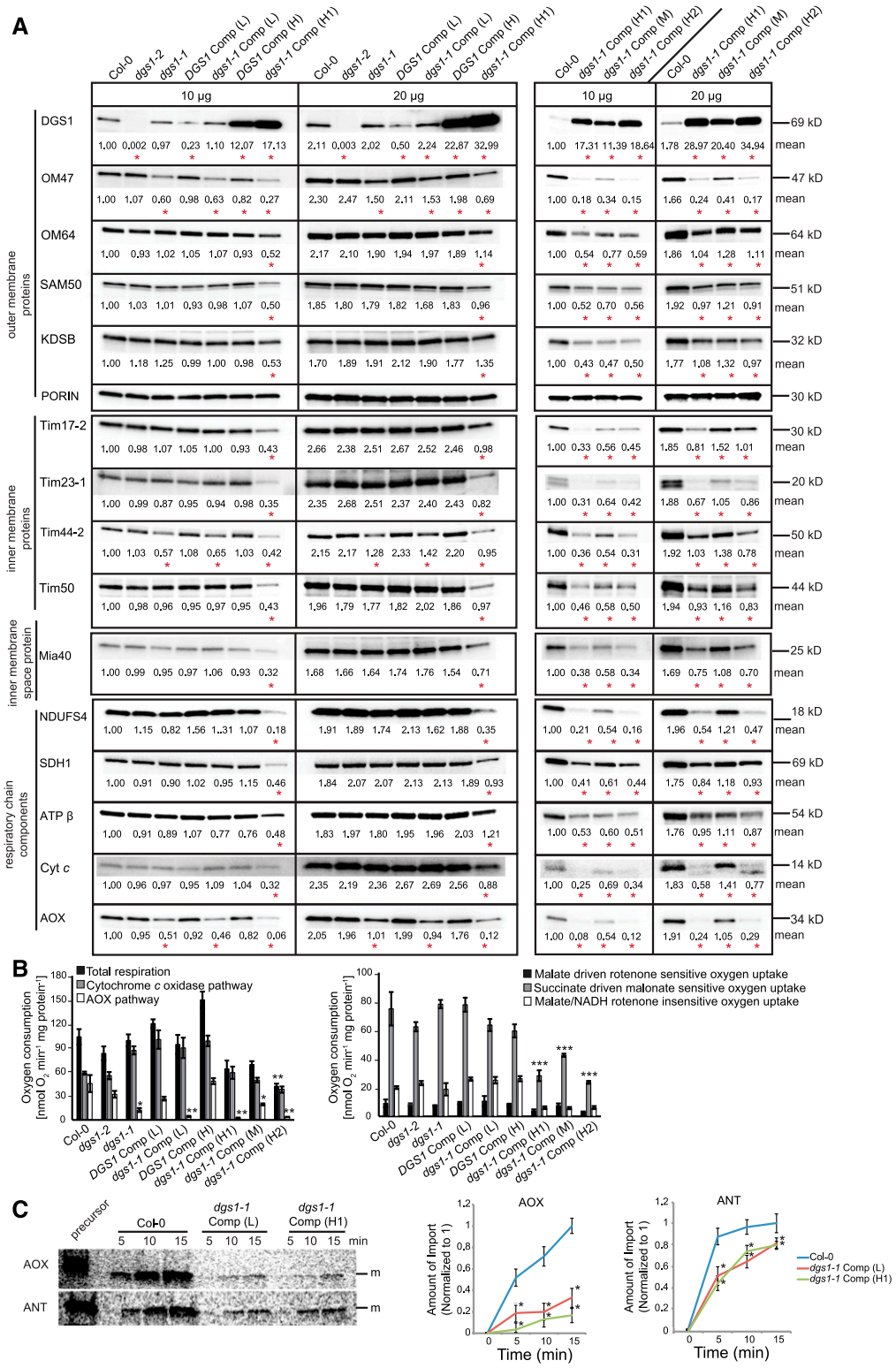

Figure 5. The *dgs1-1* Mutation Affects Mitochondrial Protein Abundance, Protein Import, and Alternative Respiratory Capacity.

(A) The protein abundance of various mitochondrial protein import components and respiratory chain components was determined by immunoblot analysis of mitochondria isolated from Col-0 and *dgs1* mutant plants. Mitochondrial proteins (10 and 20 µg) were loaded for linearity of detection. Mean values are shown for three biological replicates. P-value ≤ 0.05 from a Student's *t* test is indicated with red asterisks.

and the severity of the retarded growth phenotype was associated with the levels of the dgs1-1 mutant protein (Supplemental Figure 3). The *dgs1-1* Comp (H1) and *dgs1-1* Comp (H2) plants, which express high levels of dgs1-1 mutant protein, displayed an early senescence phenotype as evidenced by leaves losing chlorophyll after 3 weeks, a lower number of rosette leaves, and smaller inflorescences (Supplemental Figure 3). No growth defect was observed for the *dgs1-2* null allele, *DGS1* Comp (L), and *DGS1* Comp (H) plants (Supplemental Figure 3). Exposing mutant lines to drought stress revealed that *dgs1-1* and *dgs1-1* Comp (L) plants were more tolerant than Col-0, *dgs1-2*, *DGS1* Comp (L), and *DGS1* Comp (H) plants (Figure 6A). The *dgs1-1* Comp (H1) plants also displayed higher drought tolerance. To determine the underlying biochemical changes, the rosette leaves 5 to 7 were subjected to 3,3′-diaminobenzidine tetrahydrochloride (DAB) and nitroblue tetrazolium (NBT) staining to visualize the accumulation of hydrogen peroxide (H_2O_2) and superoxide radicals, respectively. The *dgs1-1*, *dgs1-1* Comp (L), and *dgs1-1* Comp (H1) lines displayed less reactive oxygen species accumulation after 8 and 10 d of drought treatment as evidenced by the lower intensity of stains (Figure 6A). After 14 d of water deprivation followed by 3 d of recovery after resupply of water, more than 80% of plants survived with *dgs1-1*, *dgs1-1* Comp (L), and *dgs1-1* Comp (H) lines, while less than 10% of the Col-0, *dgs1-2*, *DGS1* Comp (L), and *DGS1* Comp (H) plants survived (Figure 6A). Quantification of relative water content, quantum efficiency of photosystem II (F_v/F_m), total chlorophyll concentration, and CO_2fixation (Figure 6B) suggested that the plants expressing the dgs1-1 mutant protein were more effective at maintaining water content and photosynthetic efficiency during drought stress.

DAB staining of the *dgs1-1* lines revealed that the *dgs1-1* Comp (H1) plants, which displayed an early senescence phenotype (Supplemental Figure 3), contained higher levels of H_2O_2 than Col-0 plants even when not subjected to adverse (drought) conditions (Figure 6A, bottom), yet these plants displayed survival under drought compared with lines expressing the DGS1 native protein. Quantification of H_2O_2 in leaves revealed that plants with high levels of the dgs1-1 mutant protein contained higher levels of endogenous H_2O_2 (Supplemental Figure 4). This is consistent with the original identification of *dgs1-1* where overexpression resulted in growth defects and an increase of two- to threefold in H_2O_2 (Xu et al., 2008). The *dgs1-1* and *dgs1-1* Comp (L) plants, expressing lower level of dgs1-1 mutant protein, contained a similar level of H_2O_2 as Col-0 plants and did not show acceleration of dark-induced leaf senescence (Supplemental Figure 4). Thus, the amount of the dgs1-1 mutant protein present is important in determining the phenotypes observed.

To determine the underlying molecular alterations in *dgs1-1* and *dgs1-1* Comp lines, transcriptomes of the mutant and wild-type plants were analyzed by RNA sequencing (RNA-seq). The transcriptome of plants grown under nonlimiting growth conditions was not severely altered in the mutant lines, except for the complemented lines with high levels of the DGS1 wild-type protein or dgs1-1 mutant protein (Figures 7A and 7B). *DGS1* Comp (H) and *dgs1-1* Comp (H1) lines had 52 and 162 genes with altered basal expression, respectively, while all other lines had less than 10 differentially expressed genes (DEGs; fold change > 2 and false discovery rate [FDR] < 0.05) compared with the wild type (Supplemental Data Set 3). Under water-limited conditions, the transcriptome of plants containing the dgs1-1 mutant protein was different from those of the wild-type and *dgs1-2* lines complemented with the wild-type coding sequence for DGS1. Compared with the wild type that had 2230 and 2848 genes up- and downregulated by drought, plants showed a reduced number of DEGs, with 1884, 1740, and 1640 genes upregulated and 2450, 2333, and 2222 genes downregulated in *dgs1-1*, *dgs1-1* Comp (L), and *dgs1-1* Comp (H1), respectively (Figure 7A). From the total number of drought-responsive genes in the wild type, only 65%, 66%, and 55% were similarly (greater than twofold change in the same direction and FDR < 0.05) responsive in *dgs1-1*, *dgs1-1* Comp (L), and *dgs1-1* Comp (H1), respectively.

To further reveal the effect of the *dgs1-1* allele on the drought-responsive processes, genes that were commonly altered in *dgs1-1* and *dgs1-1* Comp (L) lines were analyzed as both these lines provide a readout of the effects of the *dgs1-1* allele expressed at native levels (Figure 7B; Supplemental Data Set 3). From the 720 DEGs in *dgs1-1* and *dgs1-1* Comp (L) compared with Col-0 under drought stress, three clusters could be identified that are indicated in blue, red, and green (Figure 7B). Genes in each cluster were functionally classified by Gene Ontology (GO) term enrichment analysis as indicated with the same colors (Figure 7C). Two hundred and sixty-five genes (blue cluster) were drought induced in Col-0, *dgs1-2*, *DGS1* Comp (L), and *DGS1* Comp (H), but their induction was partially or completely abolished in *dgs1-1* mutant lines (Figure 7B). These genes are associated with GO terms related to abiotic stresses such as drought, salt, H_2O_2, and cold- and stress-induced senescence, indicating that all the DGS1-1–expressing plants have largely not activated abiotic stress responses (Figure 7C). Among them are genes encoding transcription factors for drought-induced gene expression (ANAC019, ANAC072, and ANAC032), proteins involved in osmoprotection (EARLY RESPONSE TO DEHYDRATION SIX-LIKE1, ARABIDOPSIS MITOCHONDRIAL BASIC AMINO ACID CARRIER2, and LATE EMBRYOGENESIS ABUNDANT and DEHYDRIN

Figure 5. (continued).

(B) The activity of mitochondrial respiratory chain complexes from wild-type (Col-0), mutant, and Comp lines was measured using a Clark-type oxygen electrode and is shown as means ± SE of three biological replicates. Asterisks indicate the significant differences, with *P < 0.05, **P < 0.01, and ***P < 0.001 between oxygen consumption of wild-type mitochondria (Col-0) and mitochondria from different *dgs1* mutants as determined by two-way ANOVA with a post hoc Tukey's honestly significant difference test.

(C) In vitro protein import of [^{35}S]-Met-radiolabeled AOX and ANT into mitochondria isolated from Col-0 and *dgs1-1* Comp (L) plants. Aliquots were removed at 5, 10, and 15 min and then treated with protease K. (Left) A typical image of an in vitro import assay, the precursor and mature (m) forms of the protein are indicated. (Right) The rate of import was determined at all time points and normalized to Col-0 at the last time point for each replicate ($n \geq 3$). Standard errors for average ratios are indicated on graphs. Asterisks indicate the significant differences compared with Col-0 (P < 0.05, Student's *t* test).

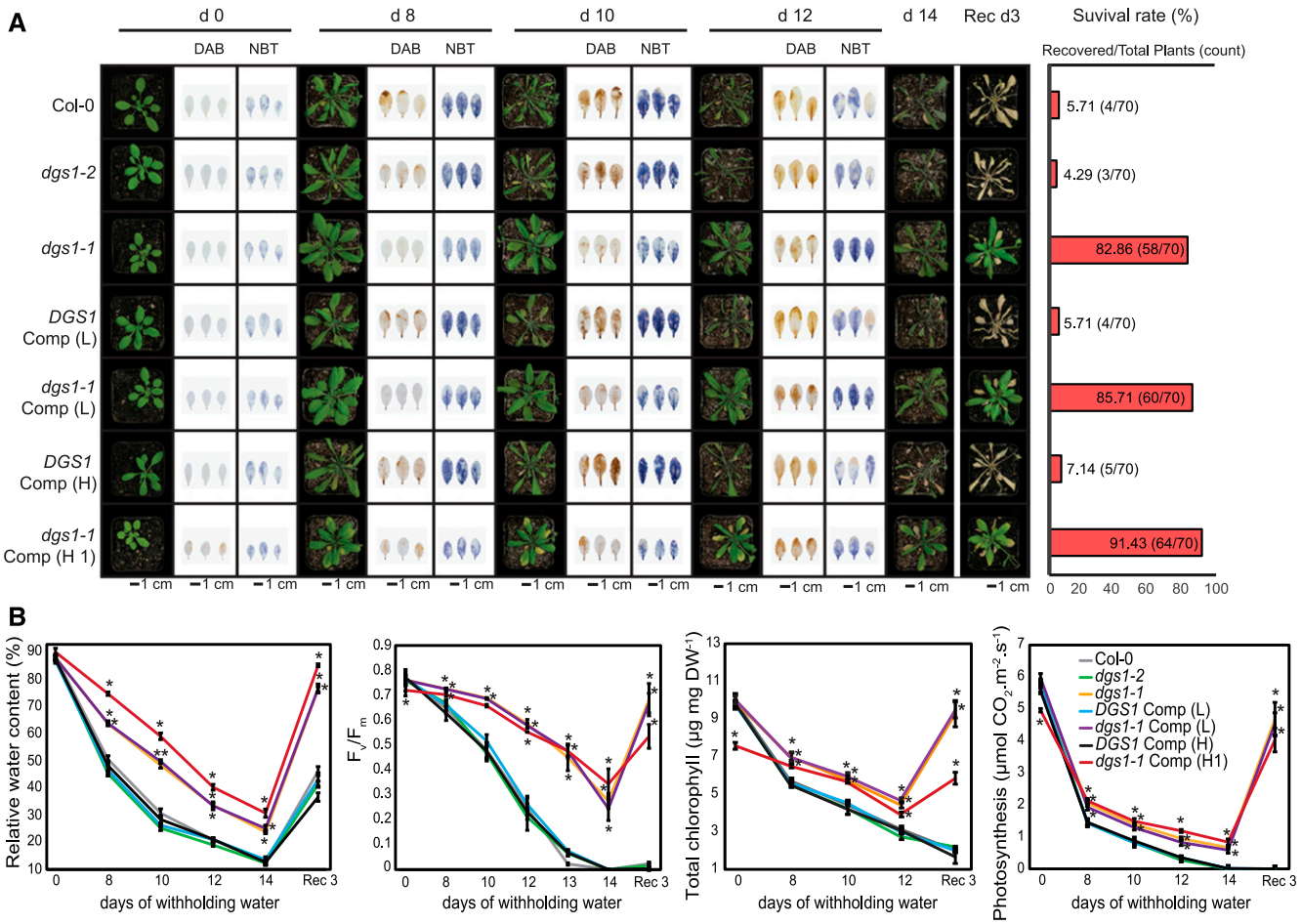

Figure 6. The *dgs1-1* Mutation Imparts Higher Drought Stress Tolerance.

(A) Wild-type (Col-0) and *dgs1* mutant lines were grown under normal conditions for 24 d and then water was withheld for 14 d followed by rewatering for 3 d to recover. Representative plants were imaged at the indicated time points. True leaves 5, 6, and 7 were harvested at the indicated time points and stained for H_2O_2 (DAB) and $O_2^{\bullet-}$ (NBT). The bar chart shows the survival ratio after 3 d of rewatering.

(B) The relative water content, maximum quantum yield (Fv/Fm), total chlorophyll content, and photosynthesis rate were measured during the drought treatment at the days as indicated. Shown are means ± SE of five biological replicates. Asterisks indicate a significant difference compared to the wild type (Col-0) at each time point ($P \leq 0.05$, Student's *t* test).

family proteins), and proteins involved in cell wall remodeling (GLYCOLIPID TRANSFER PROTEIN, XYLOGLUCAN ENDOTRANSGLUCOSYLASE/HYDROLASE, and CELLULOSE SYNTHASE family proteins). A second cluster (red) consists of 367 genes involved in photosynthesis, primary metabolism, and auxin signaling. These are downregulated in Col-0, *dgs1-2*, *DGS1* Comp (L), and *DGS1* Comp (H) plants during drought stress conditions. This redirection of energy/growth metabolism during drought stress was severely diminished in all lines expressing the mutated dgs1-1 protein, again consistent with a lack of stress response. A third cluster (green) contains genes that are upregulated in the three *dgs1-1*–expressing genotypes only. These are involved in sulfur metabolism and glucosinolate biosynthesis pathways (METHYLTHIOALKYLMALATE SYNTHASE1, METHIONINE AMINOTRANSFERASE4, CYTOCHROME P450 79F1, 3-ISOPROPYLMALATE DEHYDRATASE SMALL SUBUNIT1 and the MYB28, MYB29, and MYB76 transcription factors). Together, these data indicate that the dampened transcriptomic responses to drought stress in all genotypes expressing *dgs1-1* are attributed to the increased drought tolerance, which are probably caused by the altered physiological characteristics (e.g., lipid composition) or the ectopically expressed genes, for example,, those involved in glucosinolate biosynthesis).

Phylogenetic and Coexpression Networks of DGS1 Putative Orthologs

As DGS1 was putatively orthologous to NCA2 of yeast, a comparative analysis of their phylogeny was performed. DGS1 and NCA2 orthologs were detected in plants and fungi and in a limited number of animal groups, in Amoebozoa, Chromists, and Excavates, but not the Metazoa. The ortholog was also absent from the Alveaeolata (Figure 8A; Supplemental Data Set 4). However, the widespread presence in plants, fungi, and the Choanoflagellata

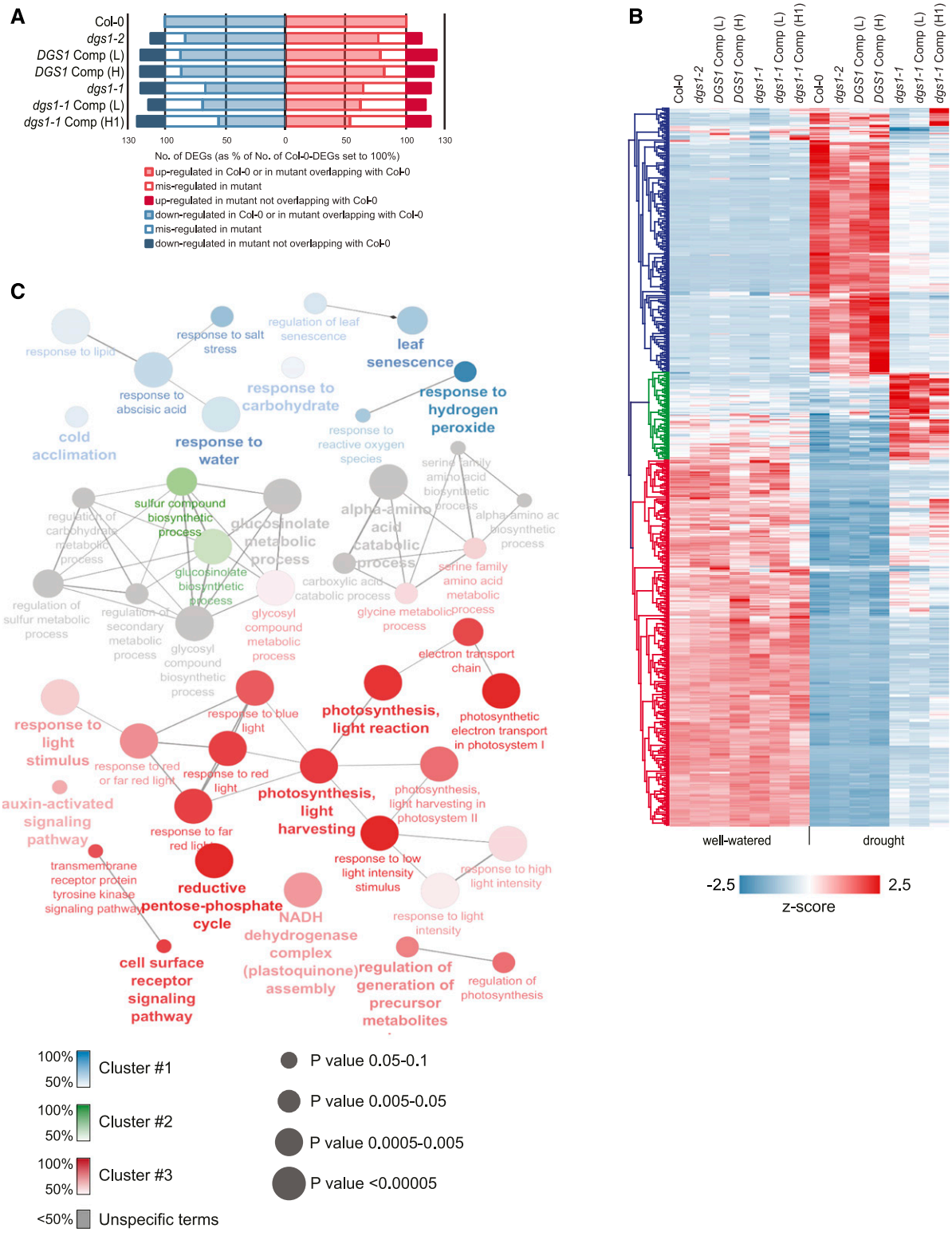

Figure 7. Transcriptome Analysis of *dgs1* Mutants.

(A) The number of upregulated genes and downregulated genes ($|\log_2$ (fold change)$|$ >1, FDR < 0.05) of each genotype leaves from plants of 24 d old plus 8-d drought treatment, compared to plants grown under normal conditions.

(*Salpingoeca rosetta*), Filasterea (*Capsaspora owcazarzaki*), and Ichthyosporea (*Sphaeroforma arctica*) suggests that DGS1and NCA2 ortholog was lost in multicellular animals.

To further explore their relationship, *DGS1* and *NCA2* were analyzed for coexpressed genes (Figure 8B; Supplemental Data Set 5). *DGS1* was strongly coexpressed with *MIC60* (15th most coexpressed genomewide), but not with *MIC10*, whereas *NCA2* was coexpressed with *MIC27*, *MIC26*, *MIC60*, and *MIC12*. Both *DGS1* and *NCA2* were coexpressed with genes related to mitochondrial fission and morphology. These included the Arabidopsis gene encoding dynamin-related GTPase DRP3B and its yeast ortholog Dnm1. Those, together with yeast mitochondrial fission 1 (Fis1), are required for mitochondrial and peroxisome fission (Otsuga et al., 1998; Bleazard et al., 1999; Mozdy et al., 2000; Fujimoto et al., 2009). Arabidopsis *drp3b* mutants and yeast *dnm1* and *fis1* mutants are defective in mitochondrial fission and display altered mitochondrial morphology, similar to the *dgs1-1* mutant. Interestingly, CLs are required for mitochondrial fission by stabilizing the Arabidopsis DRP3 oligomer complexes (Pan et al., 2014). Similarly, a functional MICOS and CLs are required for Drp1 complex stability and mitochondrial morphology in mammalian cells (Bustillo-Zabalbeitia et al., 2014; Li et al., 2016a). In addition, *DGS1* was coexpressed with *MIRO-RELATED GTP-ASE1* that is involved in mitochondrial motility and morphology, in a pathway independent of the DRP3 fission machinery (Yamaoka and Leaver, 2008; Yamaoka et al., 2011). *NCA2* was coexpressed with various genes involved in lipid metabolism and transport. For instance, the OMM protein Mitochondrial distribution and morphology34 is a core component of the ER-mitochondrial tethering complex and functions in mediating lipid import from the ER into the mitochondria (Kornmann et al., 2009). Translocator, assembly and maintenance41 (TAM41), a mitochondrial phosphatidate cytidylyltransferase, is required for CL biosynthesis (Kutik et al., 2008), and CL-specific deacylase1 is a mitochondrial CL-specific phospholipase (Beranek et al., 2009). *DGS1* was coexpressed with *PHOSPHOLIPASE D P1* that is required for extraplastidial galactolipid biosynthesis during phosphate starvation (Cruz-Ramírez et al., 2006). In addition, *NCA2*, but not DGS1, was coexpressed with genes encoding several components of the mitochondrial complex III, complex IV, and the F_1F_0-ATP synthase complex. These results showed that *DGS1* and *NCA2* were coexpressed with conserved cellular processes, indicating a similar function across phyla.

DISCUSSION

A number of lines of evidence indicate that the OMM protein DGS1 from Arabidopsis forms a multi-subunit complex that contains MIC60, a conserved core subunit of MICOS and previously identified in Arabidopsis as an important component involved in lipid trafficking in a complex called MTL (Figure 8C; Michaud et al., 2016). Consistent with our results, TOM40 and TOM20 proteins and RISP were also identified as components of MTL previously (Michaud et al., 2016), and our work establishes a link between DGS1 and this complex. We found that DGS1 represented an outer membrane component of MICOS that played a role in lipid homeostasis in plant organelles, possibly by forming contact sites with the ER and/or chloroplast/plastids to facilitate lipid import into plant mitochondria. A complete loss of the DGS1 protein in *dgs1-2* had no apparent effect on mitochondrial activity or mitochondrial protein composition and size. By contrast, the presence of the dgs1-1 mutant protein resulted in a number of alterations. At a comparable molecular level, the introduction of the dgs1-1 mutant protein resulted in decreased amounts of TOM40, TOM20, and MIC60 in this MICOS complex (Figure 2D) and weakened protease K sensitivity of MIC60 in our experiments (Figure 2C), while the increased amounts of the RISP (Figure 2D) and its increased sensitivity to protease K (Figure 2C) indicate an altered structure of the MICOS complex (Figure 8C). This is likely the consequence of the point mutation present at the intermembrane space side of the dgs1-1 protein, altering its binding affinity with these proteins (Figure 8C). Notably, a decrease in the amount of TIM44 in mitochondria was evident (Figure 5A), likely being responsible for the reduced rates of protein import observed (Figure 5C). In plants, the general mitochondrial processing peptidase is integrated into the Cyt bc_1 complex (Braun et al., 1992; Glaser et al., 1994); therefore, an increased association of the dgs1-1 mutant protein with the RISP may destabilize TIM44.

Alternatively, altered mitochondrial membrane protein abundances could be due to the altered lipid composition of mitochondria, with fewer cristae present in mitochondria that contain the dgs1-1 mutant protein (Figure 3B). The non-bilayer–forming phospholipids CL and PE are required for cristae structures and stabilization of respiratory complexes, whereas bilayer-forming phospholipid PC stabilizes TIM complexes (Schuler et al., 2016). Together, alterations in lipid composition, protein abundance, and potentially also altered mitochondria–ER contacts (hot spots for mitochondrial fission) by dysfunctional MICOS may be part of the reasons for the altered organelle size of mitochondria, chloroplasts, and the ER as evidenced by visualization with fluorescence tagging of proteins (Figure 3A). The significantly altered size of mitochondria that express the dgs1-1 mutant protein at physiological levels suggests that the balance between fusion and fission is altered in the *dgs1-1* mutant lines. This may result from an interaction of DGS1 with proteins involved in mitochondrial fusion and fission and mitochondrial dynamics (Figure 8B). Alternatively,

Figure 7. (continued).

(B) Heatmap visualization of genes differentially expressed ($|\log_2$ (fold change)$| > 1$, FDR < 0.05) in *dgs1-1* and *dgs1-1* Comp (L) compared to the wild type during drought stress conditions. Hierarchical clustering of the z-scores of $\log_2$-transformed transcripts per million values based on Euclidian distance with Genesis 1.6.0 identified three clusters (blue, green, and red).

(C) GO enrichment analysis of genes differentially expressed in *dgs1-1* and *dgs1-1* Comp (L) during drought stress conditions using ClueGO 2.5.1. The size of the nodes is proportional to the Bonferroni-corrected P-value. GO terms were grouped based on their similarity (edge thickness represents the kappa score of similarity between two GO terms), and the most significant term in each group is shown in bold. GO terms were defined as specific for one of the clusters (blue, green, or red) if the proportion of associated genes from this cluster is higher than 50%. Common GO terms are indicated in gray.

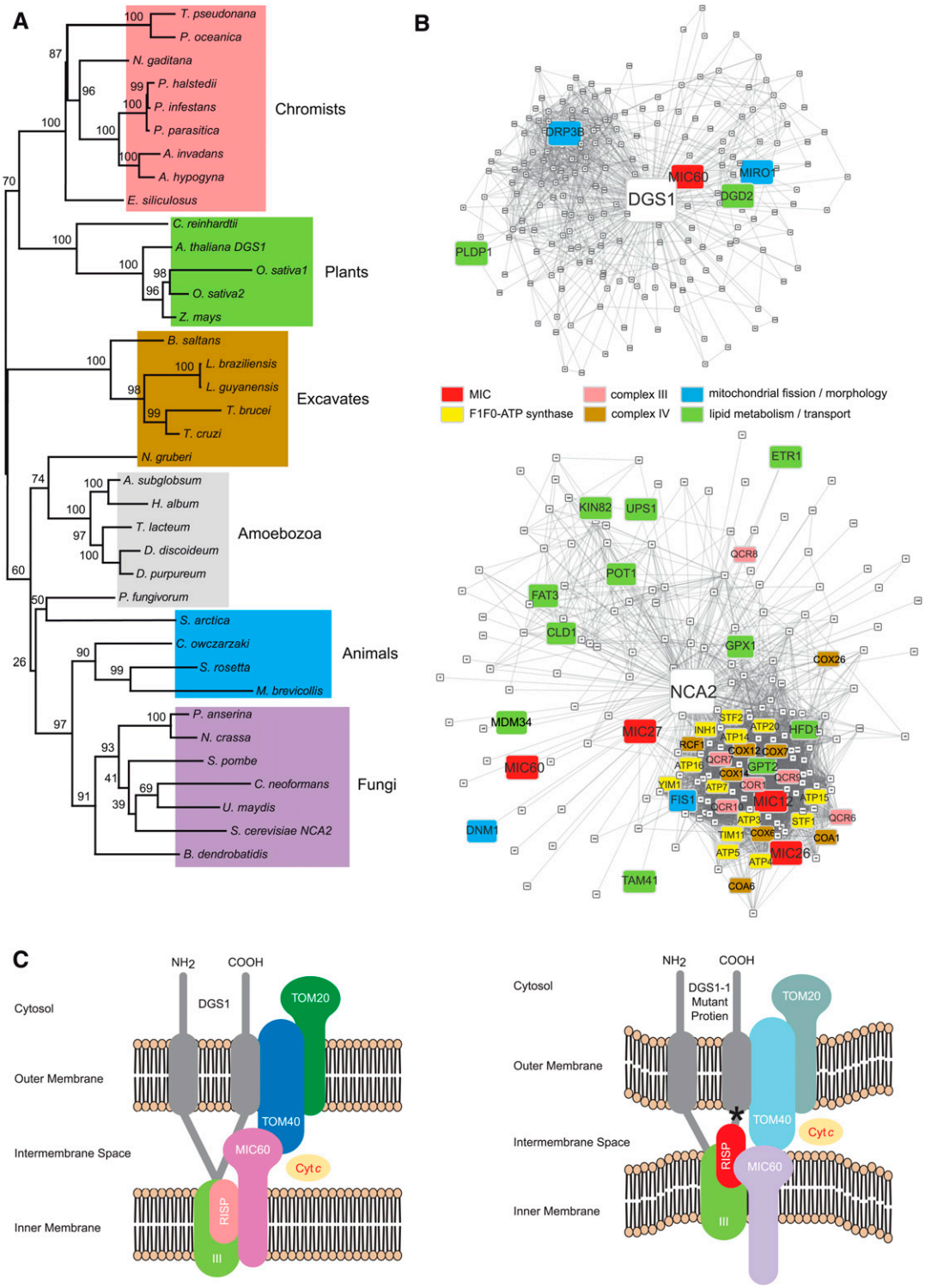

Figure 8. Phylogenetic Analysis of DGS1- and NCA2-Related Proteins.

(A) A maximum-likelihood phylogenetic tree of DGS1- and NCA2-related proteins. Numbers represent ultrafast bootstrap values after 1000 replicates from IQTREE. Some numbers have been manually moved for better visibility. The full names of species in this panel are *Nannochloropsis gaditana, Plasmopara halstedii, Phytophthora infestans, Phytophthora parasitica, Aphanomyces invadans, Achlya hypogyna, Ectocarpus siliculosus, Chlamydomonas reinhardtii, Arabidopsis thaliana, Oryza sativa, Zea mays, Bodo saltans, Leishmanian braziliensis, Leishmanian guyanensis, Trypanosoma brucei, Trypanosoma cruzi,*

CLs that were altered in *dgs1-1* mutant lines stabilize Arabidopsis DRP3 that is required for fission (Pan et al., 2014).

While the majority of DGS1 comigrated with MIC60 in complex III on BN-PAGE, it was clear that MIC60 was present in a number of other complexes, including supercomplex I+III and complexes I, F_1, and V (Figure 1A). Previously, it was reported that the MTL complex in Arabidopsis is comprised of 200 proteins, including DGS1 (Michaud et al., 2016). Thus, it is likely that the interaction of DGS1 with MIC60 is a dynamic interaction, positioning MIC60 at the interface with protein and lipid import into plant mitochondria. Notably, the impact of the dgs1-1 mutant protein on protein and lipid import into mitochondria, directly or indirectly decreasing the abundance of both TOM20s and TIM44, indicates that mitochondrial biogenesis is affected by disordering the stability or dynamics of this complex. While MIC60 and MIC10 seem to be the only subunits conserved between yeast, plants, and animals, alteration of the MICOS complex appears to have very similar impacts in all three phyla. MICOS in yeast and mammals has multifaceted effects on mitochondrial morphology, protein import and abundance, oxidative phosphorylation, and lipid synthesis (van der Laan et al., 2016; Schorr and van der Laan, 2018), which are similar to the alterations observed in this study with the expression of the dgs1-1 mutant protein.

DGS1 in plants displays sequence similarity with a yeast protein that has been called NCA2, identified in a genetic screen for genes required for the assembly/accumulation of the ATP synthase complex in yeast by yet unknown mechanisms (Pélissier et al., 1995). A comprehensive analysis of the yeast mitochondrial proteome identified it as an outer membrane protein (Zahedi et al., 2006). DGS1/NCA2 proteins are present in a wide range of eukaryotes, but they appear to have been lost in Metazoa (Figure 8A). The DGS1/NCA2-encoding genes also displayed similarities in their coexpressed genes that encode MICOS proteins, but also proteins involved in mitochondrial fission, morphology, and lipid homeostasis (Figure 8B). These proteins are conserved across kingdoms and act at mitochondria–ER contact sites where mitochondrial fission is initiated (Friedman et al., 2011). We propose that the DGS1 and NCA2 proteins play similar, but not identical, roles in yeast and plants for lipid import. This hypothesis is based on the fact that the decrease in ATP synthase in yeast is likely a secondary effect of an altered lipid composition, and CL may be a specific target that is required for the stability of the ATP synthase complex (Mehdipour and Hummer, 2016). To be noted, DGS1 and NCA2 also have specific functions. Plants carrying a homozygous null allele *dgs1-2* had no detectable alterations in plant growth or mitochondrial function. Thus, while a specific point mutation of DGS1 in *dgs1-1* resulted in an altered phenotype, a complete knockout can be compensated by other routes. This suggests that while DGS1 is part of the plant MICOS complex, import of lipids into mitochondria can still take place in the absence of the DGS1 protein. It should also be noted that it is possible that DGS1 in plants has developed additional functions needed for the complex interaction of plants with the changing environment.

AOX is a well-established marker of mitochondrial retrograde signaling (Ng et al., 2014) as it is induced upon perturbation of mitochondrial functions. An original observation for the *dgs1-1* line was that the amount of AOX in mitochondria was reduced (Moellering and Benning, 2010). Altered AOX levels are likely attributed to altered lipid membrane homeostasis and/or membrane morphology affecting protein stability. However, as AOX is typically induced by a variety of abiotic stresses (Ng et al., 2014), and the drought stress–responsive transcriptome was affected by the *dgs1-1* allele, altered signaling in *dgs1-1* mutant cannot be excluded. Although most of the altered responses represent a dampened stress response due to the increased drought tolerance of *dgs1-1* plants, a small set of genes involved in sulfur metabolism and glucosinolate biosynthesis was mis-expressed in these lines (Figure 7B). Upregulation of glucosinolate biosynthesis and metabolism has been linked to responses to drought stress (Eom et al., 2018). A positive regulator of glucosinolate metabolism in Arabidopsis, MYB29, has been previously shown to be a negative regulator of *AOX* expression (Zhang et al., 2017), and this may account for the reduction of AOX observed in the *dgs1-1* lines (Figure 5A). This supports the suggestion that there is an antagonistic relationship in the induction of glucosinolate metabolism and AOX (Zhang et al., 2017), with the former favored in the *dgs1-1* lines. Glucosinolate biosynthesis is also regulated by jasmonic acid, and there is an antagonistic interaction between the jasmonic and salicylic acid hormone signaling pathways in Arabidopsis (Thaler et al., 2012). Salicylic acid is involved in the induction of AOX, and research has indicated that this acts at the posttranscriptional level (Rhoads and McIntosh, 1992; Ho et al., 2008). Thus, the reduction in AOX may be due to altered plant hormone signaling. Additionally, the *GENOMES UNCOUPLED4* gene was greatly upregulated upon drought in the *dgs1-1* background (Figure 7B). GENOMES UNCOUPLED4 plays a regulatory role in promoting chlorophyll accumulation in response to changing environmental conditions (Larkin et al., 2003). This is consistent with the observed drought-resistant phenotype, with

Figure 8. (continued).

Naegleria gruberi, Acytostelium subglobosum, Heterostelium album, Tieghemostelium lacteum, Dictyostelium discoideum, Dictyostelium purpureum, Planoprotostelium fungivorum, Sphaeroforma arctica, Capsaspora owczarzaki, Salpingoeca rosetta, Monosiga brevicollis, Podospora anserina, Neurospora crassa, Schizosaccharomyces pombe, Cryptococcus neoformans, Ustilago maydis, Saccharomyces cerevisiae, Batrachochytrium dendrobatidis.

(B) *DGS1* and *NCA2* coexpression networks displaying the 200 top coexpressed genes.

(C) A model of the DGS1 and dgs1-1 mutant protein in plant mitochondria. For the native DGS1 protein, an ability to pull down TOM40, MIC60, and RISP along with crosslinking results suggests a direct interaction. The association with TOM20 is not defined and may be via TOM40. When dgs1-1 mutant protein was expressed, MIC60 was more protected by the inner membrane, while RISP was more exposed to the intermembrane space. The abundance of TOM40 and MIC60 was reduced in the MICOS, and the abundance of RISP was increased. The alterations of MICOS due to the presence of the dgs1-1 mutant protein may change the contact between the outer and inner membrane. The asterisk indicates the mutation site of the dgs1-1 protein.

chlorophyll concentrations and photosynthetic capacity maintained longer in *dgs1-1* mutant lines than in the wild type.

METHODS

Plant Materials

The Arabidopsis (*Arabidopsis thaliana*) DGS1 (AT5G12290) mutant *dgs1-2* (SAIL_391_F04) and *dgs1-1* alleles were described previously (Xu et al., 2008; Moellering and Benning, 2010). All Comp lines, *DGS1* Comp (L/H) with low or high expression of native DGS1 protein and *dgs1-1* Comp (L/M/H) with low, moderate, or high expression of the dgs1-1 mutant protein were generated in the null allele *dgs1-2* background by gateway cloning of the *DGS1* or *dgs1-1* coding sequence into the binary destination vector pK7WG2 and *Agrobacterium*-mediated transformation via floral dipping. The cloning primers are listed in Supplemental Data Set 6. *dgs1-1* Comp (H1) and *dgs1-1* Comp (H2) are two individual complementation lines with high but nearly equal levels of dgs1-1 mutant protein. The mutants and Comp lines were confirmed by quantification of the DGS1 or dgs1-1 mutant protein.

Plant Growth and Treatments

For normal conditions, Arabidopsis plants were grown in growth chambers at 22°C under 100 μmol m^{-2} s^{-1} light (color code 840, light color 4000K – cool white, 5240 lumen and 150-cm-long Philips Master TL-D 56 W/840 RefleX) in a 16-h light/8-h dark photoperiod. Seeds were sterilized and sown on Gamborg's B5 medium (PhytoTechnology, Austratec) supplemented with 3% (m/v) Suc, 0.43 g/L Gamborg's B5 salts (Austratec), 2 mM MES hydrate (Sigma-Aldrich), and 0.90% (w/v) Difco agar (BD Biosciences). The pH was adjusted to 5.7. Seeds were stratified for 48 h before being transferred to growth chambers in all experiments. For soil-based phenotyping or drought treatment, all lines were grown in a randomized design on soil mix. Watering was withheld when plants were 24 d old, and plants were resupplied with water after 14 d.

Isolation of Mitochondria, Chloroplasts, and ER

Mitochondria, chloroplasts, and ER were isolated as described previously (Cline et al., 1981; Bessoule et al., 1995; Lister et al., 2007), respectively, from seedlings grown on Gamborg's B5 medium for 2 weeks. Fractions were stored at −80°C and maintained on ice when in use.

Blue-Native PAGE

Twenty micrograms of mitochondria was solubilized in 2 μL of 5% (w/v) digitonin and separated on a NativePAGE Novex 4% to 16% Bis-Tris Gel (Life Technology). One-dimensional BN-PAGE was performed as described previously (Eubel et al., 2005). Following separation, gels were fixed and stained with Coomassie colloidal dye (Bio-Rad) or transferred to a polyvinylpyrrolidone membrane followed by immunodetection with the antibodies of DGS1, MIC60, TOM40, RISP, and COXII as detailed in Supplemental Data Set 7.

Immunoprecipitation

Two hundred micrograms of mitochondrial proteins was solubilized and immunoprecipitated using an Immunoprecipitation Kit (Protein A, Roche). Sample buffer was added after wash, and denaturing of proteins was achieved by heating to 100°C for 3 min followed by 30-s centrifugation at 12,000 RCF at 25°C to release proteins from beads. Samples were resolved by SDS-PAGE, transferred to a nitrocellulose membrane, and immunodetected with the antibodies of DGS1 and MIC60 as detailed in Supplemental Data Set 7.

Crosslink Assay

Protein crosslinking using DSG was performed according to manufacturer's instructions (Thermo Scientific). One milligram of freshly isolated mitochondria from the 2-week-old, water-cultured Arabidopsis wild-type and mutant plants was precipitated by centrifugation at 17,500 RCF at 4°C for 2 min and resuspended with PBS buffer (100 mM sodium phosphate and 0.15 M NaCl, pH 7.2) to a final concentration of 2 μg/μL. The samples were subsequently incubated with 5 mM DSG-PBS buffer. Samples were placed on ice for 2 h and quenched with 1 M Tris-HCl, pH 7.5, for 15 min at room temperature. Centrifugation at 500 RCF at 4°C for 2 min was performed to pellet and remove aggregated proteins. The supernatant was kept for further analysis by SDS-PAGE and immunodetection.

Generation of the DGS1 Antibody

The fragment of the DGS1 protein (amino acids 75 to 297) before the first predicted transmembrane-spanning domain was cloned by PCR reactions using the primers listed in Supplemental Data Set 6, cloned into the Gateway pDEST17 vector (Invitrogen), and transformed into the *Escherichia coli* BL21-AI (DE3) expression strain according to the manufacturer's instructions (Invitrogen). A single colony was cultured in 50 mL of Luria-Bertani medium containing 50 μg mL^{-1} carbenicillin, 0.1% (m/v) Glc, and 0.05% (m/v) L-Ara with shaking overnight at 37°C until the OD_{600} reached 0.6 to 1.0. Afterwards, 950 mL of fresh Luria-Bertani medium was inoculated and cells were grown with shaking until the OD_{600} reached 0.4. Protein expression was induced with 1.0 mM isopropyl-β-D-thiogalactopyranoside, and the cell culture was harvested after 3 h of incubation by centrifugation at 8000 RCF at 4°C for 20 min. Cells were resuspended in 50 mL of wash buffer (50 mM KH_2PO_4, 300 mM KCl, and 5 mM imidazole, pH 8.0) and lysed by sonication. The protein was purified by denaturing immobilized metal affinity chromatography using the Profinia protein purification system (Bio-Rad). Three aliquots of 200 μg of purified protein were used for injection into rabbits (WEHI), and the serum was tested by immunoblot.

Immunoblot Analysis

Proteins of different cell fractions were resolved by SDS-PAGE and transferred to a Hybond-C extra nitrocellulose membrane. Immunodetections were performed as described previously (Wang et al., 2012). The antibodies used in this study are listed in Supplemental Data Set 7. The intensities of bands of interest were quantified using Image Lab software (Bio-Rad) and calculated relative to the wild type. Three biological replicates were performed. Significant difference was determined using a Student's *t* test, and $P \leq 0.05$ is indicated by asterisks or numbers in red. Antibodies used in this study are listed in Supplemental Data Set 7.

Outer Membrane–Ruptured Mitochondria Preparation and Protease Treatment

Two hundred micrograms of freshly isolated mitochondria was precipitated, and the pellet was gently resuspended in 20 μL of SHE buffer (250 mM Suc, 1 mM EDTA, and 10 mM HEPES-KOH, pH 7.4) and incubated on ice for 15 min after mixing with 310 μL of 20 mM HEPES-KOH, pH 7.4. Following incubation, 50 μL of 2 M Suc and 20 μL of 3 M KCl were added to rupture the outer membrane. Equal amounts of outer membrane–ruptured mitochondria and intact mitochondria were incubated for 30 min on ice with 0 to 2 mg/mL protease K, and 4 μL of 100 mM phenylmethylsulfonyl fluoride was added to terminate the reaction. Samples were precipitated by centrifugation at 13,000 RCF at 4°C for 3 min and resuspended in 100 μL of SDS-PAGE sample buffer (10% [m/v] SDS, 1% [v/v] β-mercaptoethanol, 18.75% [v/v] glycerol, 0.1% [m/v] bromophenol blue, and 150 mM Tris-HCl, pH 6.8). Ten microliters of each sample was used for SDS-PAGE and immunodetection.

Protoplast Preparation and Fluorescence Microscopy

Protoplasts were isolated from the true leaves of 4-week-old Arabidopsis plants using the Tape-Arabidopsis Sandwich methods as described previously (Wu et al., 2009). A mixture of protoplasts (2 to 5 $\times$ 10^5 cells/mL) and 20 μg of plasmid DNA was incubated with 0.2 mL of 40% (m/v) polyethylene glycol 4000 at room temperature for 20 min, precipitated at 100 RCF for 1 min, and resuspended with 1 mL of W5 solution. Washes were repeated twice, and protoplasts were incubated in the dark at 19 to 20°C overnight. Fluorescence imaging was performed using an LSM780 laser scanning confocal microscope (Zeiss) with an LD C-Apochromat 40$\times$/1.1 water or 100$\times$/1.4 oil-immersion objective in multi-track channel mode. Image processing was performed using ZEN 2.3 (blue edition, Carl Zeiss Microscopy).

Electron Microscopy

Leaf tissue samples were cryofixed using an EM ICE high pressure freezer (Leica Microsystems) followed by freeze substitution in 1% osmium tetroxide in acetone for 72 h at −85°C. The samples were then slowly warmed to room temperature over the course of 24 h. The fixative was removed, and samples were washed three times with acetone before infiltration and embedding with Spurr's epoxy resin. Thin (70-nm) sections were cut using a UC7 microtome (Leica Microsystems), and the samples were imaged using a BioTwin CM120 or FEI Spirit transmission electron microscope (Thermo Fisher Scientific).

Lipid Extractions and Analysis

Lipids were extracted from isolated Arabidopsis mitochondria and chloroplasts and prepared for gas–liquid chromatography (GLC) following Wang and Benning (2011). Mitochondrial phospholipids were separated using a silica thin layer chromatography plate treated with 2.3% boric acid and a chloroform:ethanol:water:triethylamine solvent system (30:35:7:35, v/v). Lipid bands were visualized with a nondestructive primuline stain. Chloroplast polar lipids were separated using a silica thin layer chromatography plate (Si250 with preadsorbent layer, Mallinckrodt Baker) treated with $(NH_4)_2SO_4$ and an acetone:toluene:water (91:30:7, v/v) solvent system. Lipid bands were visualized with brief iodine vapor staining. Individual lipids were scraped, and their fatty methyl ester profiles were analyzed using GLC (Xu et al., 2003).

Measurements of Respiratory Parameters on Plant Mitochondria

Oxygen uptake by isolated mitochondria was measured as described previously (Jacoby et al., 2015), using a Clark-type O_2 electrode (Hansatech). Oxygen consumption driven by NADH oxidation was measured by adding malate (5 mM) and NADH (1 mM). Malate generates NADH in the mitochondrial matrix via oxidation of malate in the tricarboxylic acid cycle, and added NADH can be oxidized by the alternative external NADH dehydrogenases (Palmer and Passam, 1971; Coleman and Palmer, 1972; Palmer and Ward, 1985). Rotenone (5 μM) was added to specifically inhibit complex I to determine complex I NADH-driven oxygen consumption, and the activity remaining after rotenone addition represents oxygen consumption driven by the internal and external NADH dehydrogenases. Complex II–driven oxygen consumption was assessed by adding succinate (5 mM) and assessing the malonate (5 mM)-sensitive oxygen consumption rate, with malonate acting as a complex II inhibitor. Activity of the Cyt *c* oxidase pathway was measured in a 1-mL reaction volume of aerated respiration medium containing 0.3 M Suc, 5 mM KH_2PO_4, 10 mM TES, 10 mM NaCl, 2 mM $MgSO_4$, and 0.1% (w/v) BSA, pH 7.2, in the presence of saturating concentrations of succinate (5 mM) and NADH (1 mM), ATP (0.5 mM), ADP (0.3 mM), malate (10 mM), pyruvate (10 mM), CoA (12 μM), thiamine pyrophosphate (0.2 mM), and NAD^+ (2 mM). Potassium cyanide (1 mM) and *n*-propyl gallate (0.5 mM) were used to inhibit complex IV and AOX, respectively.

Data were analyzed based on three biological replicates. Statistical evaluations were conducted by means of two-way ANOVA with post hoc Tukey's honestly significant difference test integrated in Prism 7 (GraphPad Software). Differences with P-value < 0.05, P-value < 0.01, and P-value < 0.001 were considered as significant and indicated as *, **, and ***, respectively.

In Vitro Mitochondrial Protein Import

[^{35}S]-Met–labeled precursor proteins were synthesized and imported into freshly isolated mitochondria as described previously (Lister et al., 2007). Equal quantities of mitochondria from different genotypes were used for import reactions. Following import, mitochondria were precipitated at 20,000 RCF for 5 min and subjected to SDS-PAGE. Gels were stained in Coomassie Brilliant Blue R 250, dried, and exposed to a BAS TR2040 phosphor-imaging plate (Fuji) for 24 h. The exposed plate was visualized using the BAS 2500 Bio-Imaging Analyzer (Fuji).

In Situ Detection of Reactive Oxidative Species

Detection of H_2O_2 by DAB staining was performed as described previously (Förster et al., 2005), and reactive oxygen species in the form of $O_2^{\bullet-}$ were determined by staining with nitroblue tetrazolium as described previously (Sedigheh et al., 2011). Detached leaves were incubated in freshly prepared 1 mg/mL DAB solution, pH 7.0, or 600 μM NBT solution, pH 7.0, at room temperature in the dark (DAB stain, 8 h; NBT stain, 4 h) and then transferred to destaining solution (ethanol:acetic acid, 3:1, v/v) to remove the chlorophyll. The bleaching solution was changed every 12 h until all chlorophyll II was removed. Leaves were fixed in 50% (v/v) glycerol and scanned. Three leaves (true leaves 5, 6, and 7) per plant and three plants per genotype were assayed for both H_2O_2 and $O_2^{\bullet-}$ detection.

Dark-Induced Senescence

Arabidopsis plants were grown on soil in growth chambers at 22°C under 100 μmol m^{-2} s^{-1} light intensity in a 16-h light/8-h dark photoperiod. For dark-induced senescence, the true leaves 6 and 7 from 3-week-old Arabidopsis plants were covered with foil for 5 d. The control plants were not covered with foil and were kept growing in a 16-h light/8-h dark photoperiod.

Quantification of H_2O_2

H_2O_2 was quantified as described previously (Liu et al., 2010), using leaf extracts from 3-week-old plants. The extract was diluted accordingly and then used for H_2O_2 determination with an Amplex Red Hydrogen Peroxide/Peroxidase Assay Kit (Thermo Fisher Scientific). The values were obtained from three biological replicates, and each replicate was a pooled sample of the sixth and seventh leaves from one plant. The data were analyzed by ANOVA, and means were compared using a Student's *t* test.

Relative Water Content Analysis

The relative water content of each genotype was measured as described previously (Giraud et al., 2008). Five biological replicates were measured for each genotype, and each replicate contained the whole rosette leaves from one plant. Student's *t* test was performed to determine significant differences ($P \leq 0.05$).

Chlorophyll Analysis and Fluorescence

The total chlorophyll content was measured as described previously (Li et al., 2016b). The chlorophyll fluorescence F_v/F_m (maximum quantum yield

of PSII) was pulsed with 120 μmol m^{-2} s^{-1} of actinic light using the IMAGING-PAM M-series Chlorophyll Fluorescence System (Walz) after a 20 min of dark acclimation as described previously (Rossel et al., 2006). At least three biological replicates were measured for each genotype, and each replicate was a pooled sample of true leaves 5, 6, and 7 from one plant. Student's *t* test was performed to determine significant differences ($P \leq 0.05$).

Gas Exchange

Individual leaves were enclosed in a 1-cm reach chamber (6400-15, Li-COR) that was attached to a Li-COR portable photosynthesis system (BioScientific) according to Li et al. (2014), with some modifications. Net photosynthetic CO_2 fixation rate was measured at 22°C under 400 μmol m^{-2} s^{-1} PPFD RGB light source (6400-18A, Li-COR), 400 μmol mol^{-1} CO_2 concentration, and 65 to 75% relative humidity. The rate of respiration was determined by measuring the net photosynthetic CO_2 fixation rate in darkness. The true leaves 5, 6, and 7 from each plant, and five plants from each genotype were measured. Student's *t* test was performed to determine significant differences ($P \leq 0.05$).

Total RNA Preparation and cDNA Synthesis

Total RNA was isolated in biological triplicates from pooled 5, 6, and 7 true leaves from 3-week-old plants using the Sigma Spectrum plant total RNA isolation kit (Sigma-Aldrich) according to manufacturer's instructions. On-column DNase treatment was performed to remove genomic DNA (Thermo Fisher Scientific). The cDNA was synthesized using the iScript cDNA Synthesis Kit (Bio-Rad) according to the manufacturer's instructions.

Global Transcript Analysis

Total RNA was isolated in biological triplicates from pooled 5, 6, and 7 true leaves of well-watered and 8-d-drought-treated wild-type (Col-0) and mutant plants after growth under normal conditions for 3 weeks. RNA isolation was performed using the RNeasy Plant Mini Kit and DNA was removed via on-column DNase digestion using the RNase-Free DNase Kit (Qiagen) according to the manufacturer's instructions. The RNA was eluted in molecular grade DNase- and RNase-free water, and the integrity was validated using a TapeStation 2200 system (Agilent). RNA-seq libraries were prepared using the TruSeq Stranded mRNA Library Prep Kit (Illumina) according to the manufacturer's instructions and sequenced on a HiSeq1500 system (Illumina) as 60-bp reads or on a NextSeq550 system as 75-bp reads with an average quality score (Q30) of above 95%.

The raw reads (on average, 19.7 M per sample) were quality controlled by FastQC 0.11.5 (https://www.bioinformatics.babraham.ac.uk/projects/fastqc/) and trimmed by Trim Galore 0.4.5 (https://github.com/FelixKrueger/TrimGalore). Clean reads were pseudo aligned to the representative transcript models of the Arabidopsis Araport 11 annotation (Cheng et al., 2017) using Kallisto 0.43.1 to generate transcript per million/counts tables (Bray et al., 2016). Next, glmFit function in edgeR (Robinson et al., 2010) was used to fit the negative binomial generalized linear model (GLM) and glmLRT was used to carry out the likelihood ratio test. Differentially expressed genes were identified with a threshold of fold change > 2 and FDR < 0.05.

For the GO enrichment analyses, the Cytoscape 3.5.1 (Shannon et al., 2003) plug-in ClueGO (Bindea et al., 2009) was used. CluoGO was run with default settings, except for setting the P-value cutoff < 0.1, GO tree interval level to 4 to 9, and ≥3 or more genes from either cluster associated to a GO term, representing ≥4% (for clusters blue and red) or ≥2% (for cluster green) of the associated GO term genes. All sequencing data have been submitted to the National Center for Biotechnology Information Sequence Read Archive under project ID PRJNA475427.

Mass Spectrometry

Preparation of Samples from BN Gel Bands

Individual samples were excised from BN gels and destained (50 mM ammonium bicarbonate:acetonitrile [ACN]) overnight. Proteins were reduced in 1 μL of 200 mM tris(2-carboxyethyl)phosphine in 100 μL of water for 1 h. After washing the gel bands (50 mM ammonium bicarbonate:ACN), samples were alkylated with 4 μL of 1 M iodoacetamide in 100 μL of water for 30 min in the dark. Proteins were then digested with trypsin (0.2 μg trypsin [Promega Sequencing Grade] for 16 h at 37°C), and peptides were collected after extraction (70% ACN:water).

Liquid Chromatography-Tandem Mass Spectrometric Analysis

Peptides were reconstituted in 0.1% (v/v) TFA and 2% (v/v) ACN and loaded onto a C18 PepMap 100 μm i.d. × 2-cm trapping column (Thermo Fisher Scientific) at 5 μL/min for 6 min and washed for 6 min before switching the pre-column in line with the analytical column (PepMap RSLC C18, 2 μm, 75 μm i.d. × 25 cm; Thermo Fisher Scientific). Peptides were loaded and separated for 60 min. The separation was performed at 250 nL/min using a nonlinear ACN gradient of buffer A (0.1% [v/v] formic acid and 2% [v/v] ACN) and buffer B (0.1% [v/v] formic acid and 80% [v/v] ACN), starting at 5% (v/v) buffer B to 55% (v/v) over 55 min and then 100% (v/v) buffer B for 5 min followed by an equilibration step of 15 min (0.1% [v/v] formic acid and 2% [v/v] ACN). Data were acquired using the Xcalibur 4.1 (Thermo Fisher Scientific). The mass spectrometer was programmed to acquire in a data-dependent mode using a maximum ion injection time of 50 ms A. Full scans were acquired in the Orbitrap mass analyzer with a resolution of 120,000 at m/z 200 (3E6 ions were accumulated) from m/z 350 to 1500. The top 10 intense ions with charge states ≥ 2 were sequentially isolated to a target value of 1E5 (maximum injection time of 110 ms), fragmented by Higher-energy collisional dissociation (normalized collision energy 28%) and detected in the Orbitrap at R = 15,000, m/z 200.

Data Analysis

Identification and isotopic quantification of proteins were performed on raw output files from liquid chromatography-electrospray ionization-tandem mass spectrometry using MaxQuant 1.5.8.3 (Cox et al., 2011) together with its built-in search engine Andromeda. Carbamidomethylation of Cys was set as a fixed modification, and acetylation of protein N termini and Met oxidation were included as variable modifications. For quantitative analysis, dimethyl labeled DimethlyLys0, DimethylNter0, DimethlyLys4, DimethylNter4, DimethlyLys8, and DimethylNter8 were used as labels together with the optional intensity-based absolute quantification calculation. Parent mass tolerance was set to 4.5 ppm (after refinement by MaxQuant), and fragment mass tolerance was set to 20 ppm. Trypsin was set as the digestion enzyme with up to two missed cleavages allowed. The match between runs feature of MaxQuant was used to transfer peptide identifications from one run to another based on retention time and mass-to-charge ratio. Both peptide and protein identifications were reported at a FDR of 1%. MaxQuant was used for quantitation of labeled peptides and the calculation of normalized protein ratio.

Phylogenetic Analysis

Amino acid sequences for DGS1- or NCA2-related proteins were obtained by BLAST searches using either the yeast NCA2 or Arabidopsis DGS1 against the species listed in Supplemental Data Set 4A (Altschul et al., 1990). Full-length amino acid sequences were aligned using Clustal Omega (Li et al., 2015), and gaps were removed using TrimAl with the gappyout algorithm (Supplemental Data Set 4B; Capella-Gutiérrez et al., 2009). The resulting sequence alignment was used to create

a maximum-likelihood phylogeny using the program IQTREE (Nguyen et al., 2015). Branch support values were gained by bootstrapping with 1000 replicates.

Coexpression Analysis

The 200 top coexpressed genes were obtained from the Genevestigator Coexpression tool using the perturbation transcriptomic data set (10,615 samples for Arabidopsis and 1771 samples for *Saccharomyces cerevisiae*). All pairwise Pearson's correlations coefficients were calculated in R, and the network was visualized in Cytoscape 3.5.1. Edges were displayed if the Pearson correlation coefficient was higher than 0.65 (*DGS1* network) or 0.75 (*NCA2* network).

Accession Numbers

Sequence data from this article can be found in the GenBank/EMBL data libraries under the following accession numbers: DGS1 (At5g12290), MIC60 (At4g39690), TOM40 (At3g20000), Tom20-2 (At1g27390), Tom20-3 (At3g27080), Tom20-4 (At5g40930), RISP (At5g13430).

Supplemental Data

Supplemental Figure 1. Intramitochondrial localization of TOM20-2 and TOM40 in Col-0 and *dgs1* mutant lines. Supports Figure 2C.

Supplemental Figure 2. Leaf Lipid analysis of the wild type and mutant lines. Supports Figures 4A and 4B.

Supplemental Figure 3. Defective growth phenotype of mutants expressing the DGS1-1 protein. Supports Figure 6A.

Supplemental Figure 4. Analyses of hydrogen peroxide in *dgs1-1* lines. Supports Figure 6A.

Supplemental Data Set 1. Mass spectrometry of Supercomplex I+III, complex I, complex V, complex III, and the F_1 sub-complex of complex V excised from BN-PAGE.

Supplemental Data Set 2. Mutant and complementation lines used in the study.

Supplemental Data Set 3. Hierarchical clustering of 720 genes differentially expressed ($|\log_2 FC| > 1$ and FDR < 0.05) in *dgs1-1* and *dgs1-1* Comp (L) compared with the wild type under drought stress conditions.

Supplemental Data Set 4. (A) List of organisms and protein accession numbers where a DGS1/NCA2 type ortholog could be detected. (B) Aligned amino acid sequences for DGS1 or NCA2 related proteins with gaps removed as outlined in "Methods."

Supplemental Data Set 5. List of the top coexpressed genes for (A) *DGS1* and (B) *NCA2*.

Supplemental Data Set 6. Primers used in this study.

Supplemental Data Set 7. List of antibodies used in this study.

ACKNOWLEDGMENTS

We thank Asha Haslem for technical assistance and the La Trobe University Genomics Platform for access to next generation sequencing equipment. Mass spectrometry was undertaken at the Proteomic Platform, La Trobe University. Electron microscopy was undertaken at the Biosciences Microscopy Unit, School of Biosciences, University of Melbourne and the RMIT Microscopy & Microanalysis Facility, RMIT University. Confocal microscopy was undertaken at LIMS Bioimaging facility, La Trobe University. We thank Juliette Jouhet for providing the MIC60 antibody. This work was supported by the Australian Research Council Centre of Excellence in Plant Energy Biology (CE140100008 to J.W.); the Fonds Wetenschappelijk Onderzoek (Postdoctoral Fellowship 12N2415N and Travel Grant for a long stay abroad 450215N to I.D.C.); a Feodor Lynen Research Fellowship (Alexander von Humboldt Foundation, Germany) to J.S; Lipid analysis was supported by the Division of Chemical Sciences, Geosciences and Biosciences, Office of Basic Energy Sciences of the U.S. Department of Energy (DE-FG02-91ER20021 to A.L. and C.B.), Michigan State University AgBioResearch, and partially supported by a fellowship from Michigan State University under the Training Program in Plant Biotechnology for Health and Sustainability (T32-GM110523 to A.L. and C.B.).

AUTHOR CONTRIBUTIONS

Y.W., I.D.C., and J.W. conceived the project. L.L. performed the experiments with X.M. contributing with physiological analyses. O.B. carried out the RNA-seq and I.D.C. analyzed the RNA-seq data and performed the coexpression analyses. A.v.d.M. carried out the electron microscopy. J.S. measured the activities of respiratory chain complexes and quantified the H_2O_2 content together with Y.W. A.L. and C.B. carried out and interpreted the lipid analysis. C.C. carried out the phylogenetic analysis. L.L. drafted the article that was edited by J.W., I.D.C., and Y.W. The final version was produced with contributions from all authors.

Received November 28, 2018; revised April 15, 2019; accepted May 9, 2019; published May 22, 2019.

REFERENCES

Aaltonen, M.J., Friedman, J.R., Osman, C., Salin, B., di Rago, J.P., Nunnari, J., Langer, T., and Tatsuta, T. (2016). MICOS and phospholipid transfer by Ups2-Mdm35 organize membrane lipid synthesis in mitochondria. J. Cell Biol. **213:** 525–534.

Altschul, S.F., Gish, W., Miller, W., Myers, E.W., and Lipman, D.J. (1990). Basic local alignment search tool. J. Mol. Biol. **215:** 403–410.

Awai, K., Maréchal, E., Block, M.A., Brun, D., Masuda, T., Shimada, H., Takamiya, K., Ohta, H., and Joyard, J. (2001). Two types of MGDG synthase genes, found widely in both 16:3 and 18:3 plants, differentially mediate galactolipid syntheses in photosynthetic and nonphotosynthetic tissues in *Arabidopsis thaliana*. Proc. Natl. Acad. Sci. USA **98:** 10960–10965.

Benning, C., and Ohta, H. (2005). Three enzyme systems for galactoglycerolipid biosynthesis are coordinately regulated in plants. J. Biol. Chem. **280:** 2397–2400.

Beranek, A., Rechberger, G., Knauer, H., Wolinski, H., Kohlwein, S.D., and Leber, R. (2009). Identification of a cardiolipin-specific phospholipase encoded by the gene CLD1 (YGR110W) in yeast. J. Biol. Chem. **284:** 11572–11578.

Bessoule, J.J., Testet, E., and Cassagne, C. (1995). Synthesis of phosphatidylcholine in the chloroplast envelope after import of lysophosphatidylcholine from endoplasmic reticulum membranes. Eur. J. Biochem. **228:** 490–497.

Bindea, G., Mlecnik, B., Hackl, H., Charoentong, P., Tosolini, M., Kirilovsky, A., Fridman, W.-H., Pagès, F., Trajanoski, Z., and Galon, J. (2009). ClueGO: A Cytoscape plug-in to decipher functionally grouped gene ontology and pathway annotation networks. Bioinformatics **25:** 1091–1093.

Bleazard, W., McCaffery, J.M., King, E.J., Bale, S., Mozdy, A., Tieu, Q., Nunnari, J., and Shaw, J.M. (1999). The dynamin-related

GTPase Dnm1 regulates mitochondrial fission in yeast. Nat. Cell Biol. **1:** 298–304.

Braun, H.P., Emmermann, M., Kruft, V., and Schmitz, U.K. (1992). The general mitochondrial processing peptidase from potato is an integral part of cytochrome c reductase of the respiratory chain. EMBO J. **11:** 3219–3227.

Bray, N.L., Pimentel, H., Melsted, P., and Pachter, L. (2016). Near-optimal probabilistic RNA-seq quantification. Nat. Biotechnol. **34:** 525–527.

Bustillo-Zabalbeitia, I., Montessuit, S., Raemy, E., Basañez, G., Terrones, O., and Martinou, J.C. (2014). Specific interaction with cardiolipin triggers functional activation of Dynamin-Related Protein 1. PLoS One **9:** e102738.

Camougrand, N., Pélissier, P., Velours, G., and Guérin, M. (1995). NCA2, a second nuclear gene required for the control of mitochondrial synthesis of subunits 6 and 8 of ATP synthase in *Saccharomyces cerevisiae.* J. Mol. Biol. **247:** 588–596.

Capella-Gutiérrez, S., Silla-Martínez, J.M., and Gabaldón, T. (2009). trimAl: A tool for automated alignment trimming in large-scale phylogenetic analyses. Bioinformatics **25:** 1972–1973.

Carrie, C., Giraud, E., and Whelan, J. (2009). Protein transport in organelles: Dual targeting of proteins to mitochondria and chloroplasts. FEBS J. **276:** 1187–1195.

Cheng, C.Y., Krishnakumar, V., Chan, A.P., Thibaud-Nissen, F., Schobel, S., and Town, C.D. (2017). Araport11: A complete reannotation of the *Arabidopsis thaliana* reference genome. Plant J. **89:** 789–804.

Cline, K., Andrews, J., Mersey, B., Newcomb, E.H., and Keegstra, K. (1981). Separation and characterization of inner and outer envelope membranes of pea chloroplasts. Proc. Natl. Acad. Sci. USA **78:** 3595–3599.

Coleman, J.O.D., and Palmer, J.M. (1972). The oxidation of malate by isolated plant mitochondria. Eur. J. Biochem. **26:** 499–509.

Cox, J., Neuhauser, N., Michalski, A., Scheltema, R.A., Olsen, J.V., and Mann, M. (2011). Andromeda: A peptide search engine integrated into the MaxQuant environment. J. Proteome Res. **10:** 1794–1805.

Cruz-Ramírez, A., Oropeza-Aburto, A., Razo-Hernández, F., Ramírez-Chávez, E., and Herrera-Estrella, L. (2006). Phospholipase DZ2 plays an important role in extraplastidic galactolipid biosynthesis and phosphate recycling in Arabidopsis roots. Proc. Natl. Acad. Sci. USA **103:** 6765–6770.

Duchêne, A.M., Giritch, A., Hoffmann, B., Cognat, V., Lancelin, D., Peeters, N.M., Zaepfel, M., Maréchal-Drouard, L., and Small, I.D. (2005). Dual targeting is the rule for organellar aminoacyl-tRNA synthetases in *Arabidopsis thaliana*. Proc. Natl. Acad. Sci. USA **102:** 16484–16489.

Elo, A., Lyznik, A., Gonzalez, D.O., Kachman, S.D., and Mackenzie, S.A. (2003). Nuclear genes that encode mitochondrial proteins for DNA and RNA metabolism are clustered in the Arabidopsis genome. Plant Cell **15:** 1619–1631.

Eom, S. H., Baek, S. A., Kim, J. K., and Hyun, T. K. (2018). Transcriptome analysis in Chinese cabbage (*Brassica rapa* ssp. *pekinensis*) provides the role of glucosinolate metabolism in response to drought stress. Molecules **23:** 1186.

Eubel, H., Braun, H.-P., and Millar, A.H. (2005). Blue-native PAGE in plants: A tool in analysis of protein-protein interactions. Plant Methods **1:** 11.

Förster, B., Osmond, C.B., and Pogson, B.J. (2005). Improved survival of very high light and oxidative stress is conferred by spontaneous gain-of-function mutations in Chlamydomonas. Biochim. Biophys. Acta **1709:** 45–57.

Friedman, J.R., Lackner, L.L., West, M., DiBenedetto, J.R., Nunnari, J., and Voeltz, G.K. (2011). ER tubules mark sites of mitochondrial division. Science **334:** 358–362.

Fujimoto, M., Arimura, S., Mano, S., Kondo, M., Saito, C., Ueda, T., Nakazono, M., Nakano, A., Nishimura, M., and Tsutsumi, N. (2009). Arabidopsis dynamin-related proteins DRP3A and DRP3B are functionally redundant in mitochondrial fission, but have distinct roles in peroxisomal fission. Plant J. **58:** 388–400.

Giraud, E., Ho, L.H., Clifton, R., Carroll, A., Estavillo, G., Tan, Y.F., Howell, K.A., Ivanova, A., Pogson, B.J., Millar, A.H., and Whelan, J. (2008). The absence of ALTERNATIVE OXIDASE1a in Arabidopsis results in acute sensitivity to combined light and drought stress. Plant Physiol. **147:** 595–610.

Glaser, E., Eriksson, A., and Sjöling, S. (1994). Bifunctional role of the bc1 complex in plants. Mitochondrial bc1 complex catalyses both electron transport and protein processing. FEBS Lett. **346:** 83–87.

Härtel, H., Dormann, P., and Benning, C. (2000). DGD1-independent biosynthesis of extraplastidic galactolipids after phosphate deprivation in Arabidopsis. Proc. Natl. Acad. Sci. USA **97:** 10649–10654.

Ho, L.H., Giraud, E., Uggalla, V., Lister, R., Clifton, R., Glen, A., Thirkettle-Watts, D., Van Aken, O., and Whelan, J. (2008). Identification of regulatory pathways controlling gene expression of stress-responsive mitochondrial proteins in Arabidopsis. Plant Physiol. **147:** 1858–1873.

Jacoby, R.P., Millar, A.H., and Taylor, N.L. (2015). Assessment of respiration in isolated plant mitochondria using Clark-type electrodes. Methods Mol. Biol. **1305:** 165–185.

Jouhet, J., Maréchal, E., Baldan, B., Bligny, R., Joyard, J., and Block, M.A. (2004). Phosphate deprivation induces transfer of DGDG galactolipid from chloroplast to mitochondria. J. Cell Biol. **167:** 863–874.

Kelly, A.A., and Dörmann, P. (2002). DGD2, an arabidopsis gene encoding a UDP-galactose-dependent digalactosyldiacylglycerol synthase is expressed during growth under phosphate-limiting conditions. J. Biol. Chem. **277:** 1166–1173.

Kornmann, B., Currie, E., Collins, S.R., Schuldiner, M., Nunnari, J., Weissman, J.S., and Walter, P. (2009). An ER-mitochondria tethering complex revealed by a synthetic biology screen. Science **325:** 477–481.

Kozjak-Pavlovic, V. (2017). The MICOS complex of human mitochondria. Cell Tissue Res. **367:** 83–93.

Kutik, S., Rissler, M., Guan, X.L., Guiard, B., Shui, G., Gebert, N., Heacock, P.N., Rehling, P., Dowhan, W., Wenk, M.R., Pfanner, N., and Wiedemann, N. (2008). The translocator maintenance protein Tam41 is required for mitochondrial cardiolipin biosynthesis. J. Cell Biol. **183:** 1213–1221.

Larkin, R.M., Alonso, J.M., Ecker, J.R., and Chory, J. (2003). GUN4, a regulator of chlorophyll synthesis and intracellular signaling. Science **299:** 902–906.

Li, H., et al. (2016a). Mic60/Mitofilin determines MICOS assembly essential for mitochondrial dynamics and mtDNA nucleoid organization. Cell Death Differ. **23:** 380–392.

Li, L., Kubiszewski-Jakubiak, S., Radomiljac, J., Wang, Y., Law, S.R., Keech, O., Narsai, R., Berkowitz, O., Duncan, O., Murcha, M.W., and Whelan, J. (2016b). Characterization of a novel β-barrel protein (AtOM47) from the mitochondrial outer membrane of *Arabidopsis thaliana*. J. Exp. Bot. **67:** 6061–6075.

Li, W., Cowley, A., Uludag, M., Gur, T., McWilliam, H., Squizzato, S., Park, Y.M., Buso, N., and Lopez, R. (2015). The EMBL-EBI bioinformatics web and programmatic tools framework. Nucleic Acids Res. **43:** W580-4.

Li, X., Han, L., Zhao, Y., You, Z., Dong, H., and Zhang, C. (2014). Hpa1 harpin needs nitroxyl terminus to promote vegetative growth and leaf photosynthesis in Arabidopsis. J. Biosci. **39:** 127–137.

Lister, R., Carrie, C., Duncan, O., Ho, L.H., Howell, K.A., Murcha, M.W., and Whelan, J. (2007). Functional definition of outer membrane

proteins involved in preprotein import into mitochondria. Plant Cell **19:** 3739–3759.

Liu, Y., Ye, N., Liu, R., Chen, M., and Zhang, J. (2010). H_2O_2 mediates the regulation of ABA catabolism and GA biosynthesis in Arabidopsis seed dormancy and germination. J. Exp. Bot. **61:** 2979–2990.

Mehdipour, A.R., and Hummer, G. (2016). Cardiolipin puts the seal on ATP synthase. Proc. Natl. Acad. Sci. USA **113:** 8568–8570.

Mesmin, B. (2016). Mitochondrial lipid transport and biosynthesis: A complex balance. J. Cell Biol. **214:** 9–11.

Michaud, M., et al. (2016). AtMic60 is involved in plant mitochondria lipid trafficking and is part of a large complex. Curr. Biol. **26:** 627–639.

Michaud, M., Prinz, W.A., and Jouhet, J. (2017). Glycerolipid synthesis and lipid trafficking in plant mitochondria. FEBS J. **284:** 376–390.

Moellering, E.R., and Benning, C. (2010). Phosphate regulation of lipid biosynthesis in Arabidopsis is independent of the mitochondrial outer membrane DGS1 complex. Plant Physiol. **152:** 1951–1959.

Moellering, E.R., and Benning, C. (2011). Galactoglycerolipid metabolism under stress: A time for remodeling. Trends Plant Sci. **16:** 98–107.

Moellering, E.R., Muthan, B., and Benning, C. (2010). Freezing tolerance in plants requires lipid remodeling at the outer chloroplast membrane. Science **330:** 226–228.

Mozdy, A.D., McCaffery, J.M., and Shaw, J.M. (2000). Dnm1p GTPase-mediated mitochondrial fission is a multi-step process requiring the novel integral membrane component Fis1p. J. Cell Biol. **151:** 367–380.

Muñoz-Gómez, S.A., Slamovits, C.H., Dacks, J.B., Baier, K.A., Spencer, K.D., and Wideman, J.G. (2015a). Ancient homology of the mitochondrial contact site and cristae organizing system points to an endosymbiotic origin of mitochondrial cristae. Curr. Biol. **25:** 1489–1495.

Muñoz-Gómez, S.A., Slamovits, C.H., Dacks, J.B., and Wideman, J.G. (2015b). The evolution of MICOS: Ancestral and derived functions and interactions. Commun. Integr. Biol. **8:** e1094593.

Murcha, M.W., Kmiec, B., Kubiszewski-Jakubiak, S., Teixeira, P.F., Glaser, E., and Whelan, J. (2014). Protein import into plant mitochondria: Signals, machinery, processing, and regulation. J. Exp. Bot. **65:** 6301–6335.

Ng, S., De Clercq, I., Van Aken, O., Law, S.R., Ivanova, A., Willems, P., Giraud, E., Van Breusegem, F., and Whelan, J. (2014). Anterograde and retrograde regulation of nuclear genes encoding mitochondrial proteins during growth, development, and stress. Mol. Plant **7:** 1075–1093.

Nguyen, L.T., Schmidt, H.A., von Haeseler, A., and Minh, B.Q. (2015). IQ-TREE: A fast and effective stochastic algorithm for estimating maximum-likelihood phylogenies. Mol. Biol. Evol. **32:** 268–274.

Otsuga, D., Keegan, B.R., Brisch, E., Thatcher, J.W., Hermann, G.J., Bleazard, W., and Shaw, J.M. (1998). The dynamin-related GTPase, Dnm1p, controls mitochondrial morphology in yeast. J. Cell Biol. **143:** 333–349.

Palmer, J.M., and Passam, H.C. (1971). The oxidation of exogenous reduced nicotinamide-adenine dinucleotide by plant mitochondria. Biochem. J. **122:** 16P–17P.

Palmer, J.M., and Ward, J.A. (1985). The oxidation of NADH by plant mitochondria. In Encyclopedia of Plant Physiology, New Series, Vol. 18, Higher Plant Cell Respiration, R. Douce, and D.A. Day, eds (Berlin: Springer), pp. 73–201.

Palmer, C.S., Osellame, L.D., Stojanovski, D., and Ryan, M.T. (2011). The regulation of mitochondrial morphology: Intricate mechanisms and dynamic machinery. Cell. Signal. **23:** 1534–1545.

Pan, R., Jones, A.D., and Hu, J. (2014). Cardiolipin-mediated mitochondrial dynamics and stress response in Arabidopsis. Plant Cell **26:** 391–409.

Pélissier, P., Camougrand, N., Velours, G., and Guérin, M. (1995). NCA3, a nuclear gene involved in the mitochondrial expression of subunits 6 and 8 of the Fo-F1 ATP synthase of *S. cerevisiae*. Curr. Genet. **27:** 409–416.

Rabl, R., et al. (2009). Formation of cristae and crista junctions in mitochondria depends on antagonism between Fcj1 and Su e/g. J. Cell Biol. **185:** 1047–1063.

Rhoads, D.M., and McIntosh, L. (1992). Salicylic acid regulation of respiration in higher plants: Alternative oxidase expression. Plant Cell **4:** 1131–1139.

Robinson, M.D., McCarthy, D.J., and Smyth, G.K. (2010). edgeR: A bioconductor package for differential expression analysis of digital gene expression data. Bioinformatics **26:** 139–140.

Rose, R.J., and McCurdy, D.W. (2017). New beginnings: Mitochondrial renewal by massive mitochondrial fusion. Trends Plant Sci. **22:** 641–643.

Rossel, J.B., Walter, P.B., Hendrickson, L., Chow, W.S., Poole, A., Mullineaux, P.M., and Pogson, B.J. (2006). A mutation affecting ASCORBATE PEROXIDASE 2 gene expression reveals a link between responses to high light and drought tolerance. Plant Cell Environ. **29:** 269–281.

Schneider, A. (2011). Mitochondrial tRNA import and its consequences for mitochondrial translation. Annu. Rev. Biochem. **80:** 1033–1053.

Schorr, S., and van der Laan, M. (2018). Integrative functions of the mitochondrial contact site and cristae organizing system. Semin. Cell Dev. Biol. **76:** 191–200.

Schuler, M.H., Di Bartolomeo, F., Mårtensson, C.U., Daum, G., and Becker, T. (2016). Phosphatidylcholine affects inner membrane protein translocases of mitochondria. J. Biol. Chem. **291:** 18718–18729.

Sedigheh, H.G., Mortazavian, M., Norouzian, D., Atyabi, M., Akbarzadeh, A., Hasanpoor, K., and Ghorbani, M. (2011). Oxidative stress and leaf senescence. BMC Res. Notes **4:** 477.

Shannon, P, Markiel, A, Baliga, NS, Wang, JT, Ramage, D, Amin, N, Schwikowski, B, and Ideker, T. (2003). Cytoscape: a software environment for integrated models of biomolecular interactions networks. Genome Res. **13:** 2498–504.

Siedow, J.N., and Girvin, M.E. (1980). Alternative respiratory pathway: Its role in seed respiration and its inhibition by propyl gallate. Plant Physiol. **65:** 669–674.

Thaler, J.S., Humphrey, P.T., and Whiteman, N.K. (2012). Evolution of jasmonate and salicylate signal crosstalk. Trends Plant Sci. **17:** 260–270.

van der Laan, M., Bohnert, M., Wiedemann, N., and Pfanner, N. (2012). Role of MINOS in mitochondrial membrane architecture and biogenesis. Trends Cell Biol. **22:** 185–192.

van der Laan, M., Horvath, S.E., and Pfanner, N. (2016). Mitochondrial contact site and cristae organizing system. Curr. Opin. Cell Biol. **41:** 33–42.

Wang, Z., and Benning, C. (2011). *Arabidopsis thaliana* polar glycerolipid profiling by thin layer chromatography (TLC) coupled with gas-liquid chromatography (GLC). J. Vis. Exp. **49:** 2518.

Wang, Y., Carrie, C., Giraud, E., Elhafez, D., Narsai, R., Duncan, O., Whelan, J., and Murcha, M.W. (2012). Dual location of the mitochondrial preprotein transporters B14.7 and Tim23-2 in complex I and the TIM17:23 complex in Arabidopsis links mitochondrial activity and biogenesis. Plant Cell **24:** 2675–2695.

Wideman, J.G., and Muñoz-Gómez, S.A. (2016). The evolution of ERMIONE in mitochondrial biogenesis and lipid homeostasis: An

evolutionary view from comparative cell biology. Biochim. Biophys. Acta **1861** (8 Pt B): 900–912.

Wiedemann, N., and Pfanner, N. (2017). Mitochondrial machineries for protein import and assembly. Annu. Rev. Biochem. **86:** 685–714.

Wu, F.H., Shen, S.C., Lee, L.Y., Lee, S.H., Chan, M.T., and Lin, C.S. (2009). Tape-Arabidopsis Sandwich - A simpler Arabidopsis protoplast isolation method. Plant Methods **5:** 16.

Xu, C., Fan, J., Riekhof, W., Froehlich, J.E., and Benning, C. (2003). A permease-like protein involved in ER to thylakoid lipid transfer in Arabidopsis. EMBO J. **22:** 2370–2379.

Xu, C., Moellering, E.R., Fan, J., and Benning, C. (2008). Mutation of a mitochondrial outer membrane protein affects chloroplast lipid biosynthesis. Plant J. **54:** 163–175.

Yamaoka, S., and Leaver, C.J. (2008). EMB2473/MIRO1, an Arabidopsis Miro GTPase, is required for embryogenesis and influences mitochondrial morphology in pollen. Plant Cell **20:** 589–601.

Yamaoka, S., Nakajima, M., Fujimoto, M., and Tsutsumi, N. (2011). MIRO1 influences the morphology and intracellular distribution of mitochondria during embryonic cell division in Arabidopsis. Plant Cell Rep. **30:** 239–244.

Zahedi, R.P., Sickmann, A., Boehm, A.M., Winkler, C., Zufall, N., Schönfisch, B., Guiard, B., Pfanner, N., and Meisinger, C. (2006). Proteomic analysis of the yeast mitochondrial outer membrane reveals accumulation of a subclass of preproteins. Mol. Biol. Cell **17:** 1436–1450.

Zhang, X., et al. (2017). The transcription factor MYB29 is a regulator of *ALTERNATIVE OXIDASE1a.* Plant Physiol. **173:** 1824–1843.